Published in final edited form as:

FASEB J. 2022 October ; 36(10): e22521. doi:10.1096/fj.202200033R.

Dual near-infrared II laser modulates the cellular redox state of T cells and augments the efficacy of cancer immunotherapy

Wataru Katagiri[#],

Gordon Center for Medical Imaging, Department of Radiology, Massachusetts General Hospital, 149 13th Street, Charlestown, MA 02129, USA

Graduate School of Science and Technology, Keio University, 3-14-1 Hiyoshi, Yokohama, Kanagawa 223-8522, Japan

Shinya Yokomizo[#],

Gordon Center for Medical Imaging, Department of Radiology, Massachusetts General Hospital, 149 13th Street, Charlestown, MA 02129, USA

Department of Radiological Science, Tokyo Metropolitan University, 7-2-10 Higashi-Ogu, Arakawa, Tokyo 116-8551, Japan

Takanobu Ishizuka,

Bioresearch Center, Corporate R&D Center, Terumo Corporation, 1500 Inokuchi, Nakai-machi, Ashigarakami-gun, Kanagawa 259-0151, Japan

Corporate R&D Center, Terumo Corporation, 1500 Inokuchi, Nakai-machi, Ashigarakami-gun, Kanagawa 259-0151, Japan

Keiko Yamashita,

Corporate R&D Center, Terumo Corporation, 1500 Inokuchi, Nakai-machi, Ashigarakami-gun, Kanagawa 259-0151, Japan

Timo Kopp,

Interfaculty Institute of Biochemistry (IFIB), University of Tübingen, Auf der Morgenstelle 34, Tübingen 72076, Germany

Malte Roessing,

Interfaculty Institute of Biochemistry (IFIB), University of Tübingen, Auf der Morgenstelle 34, Tübingen 72076, Germany

[*]**Correspondence should be addressed:** Satoshi Kashiwagi, M.D., Ph.D., Gordon Center for Medical Imaging, Department of Radiology, Massachusetts General Hospital, 149 13th Street, Charlestown, MA 02129, USA, Tel: 617-726-6265; skashiwagi@mgh.harvard.edu.

[#]These authors contributed equally.

Author contributions:

W Katagiri, S Yokomizo, T Ishizuka, K Yamashita, S Kashiwagi designed the study; W Katagiri, S Yokomizo, E Ogawa designed and constructed the laser system; W Katagiri, S Yokomizo, T Fukuda, H Monaco, S Manganiello performed the immunoassays and data analysis; W Katagiri, S Yokomizo, T Fukuda, H Monaco, S Manganiello, MR Ng, D Fukumura, S Nomura, DN Atochin, HS Choi performed the laser exposure and murine cancer model studies and data analysis; W Katagiri, S Yokomizo, T Fukuda, H Monaco, S Manganiello, HS Choi performed the cell-based assays and data analysis; S Yokomizo, T Kopp, M Roessing, S Feil performed the tissue damage study and immunoblot analysis; W Katagiri, S Yokomizo, T Ishizuka, K Yamashita, A Sato, T Iwasaki, H Sato performed the histological analysis of the tumor models; W Katagiri, DN Atochin, S Kashiwagi wrote the manuscript.

Potential conflict of interest:

The authors declare no potential conflicts of interest.

Akiko Sato,
Bioresearch Center, Corporate R&D Center, Terumo Corporation, 1500 Inokuchi, Nakai-machi, Ashigarakami-gun, Kanagawa 259-0151, Japan

Taizo Iwasaki,
Bioresearch Center, Corporate R&D Center, Terumo Corporation, 1500 Inokuchi, Nakai-machi, Ashigarakami-gun, Kanagawa 259-0151, Japan

Hideki Sato,
Bioresearch Center, Corporate R&D Center, Terumo Corporation, 1500 Inokuchi, Nakai-machi, Ashigarakami-gun, Kanagawa 259-0151, Japan

Takeshi Fukuda,
Gordon Center for Medical Imaging, Department of Radiology, Massachusetts General Hospital, 149 13th Street, Charlestown, MA 02129, USA

Hailey Monaco,
Gordon Center for Medical Imaging, Department of Radiology, Massachusetts General Hospital, 149 13th Street, Charlestown, MA 02129, USA

Sophia Manganiello,
Gordon Center for Medical Imaging, Department of Radiology, Massachusetts General Hospital, 149 13th Street, Charlestown, MA 02129, USA

Shinsuke Nomura,
Gordon Center for Medical Imaging, Department of Radiology, Massachusetts General Hospital, 149 13th Street, Charlestown, MA 02129, USA

Department of Surgery, Faculty of Medicine, University of Miyazaki Hospital, 5200 Kihara, Kiyotake, Miyazaki, Miyazaki 889-1692, Japan

Mei Rosa Ng,
Edwin L. Steele Laboratory for Tumor Biology, Department of Radiation Oncology, Massachusetts General Hospital, 149 13th Street, Charlestown, MA 02129, USA

Susanne Feil,
Interfaculty Institute of Biochemistry (IFIB), University of Tübingen, Auf der Morgenstelle 34, Tübingen 72076, Germany

Emiyu Ogawa [Prof.],
School of Allied Health Science, Kitasato University, 1-15-1 Kitasato Minami-ku Sagamihara, Kanagawa, Japan

Dai Fukumura [Prof.],
Edwin L. Steele Laboratory for Tumor Biology, Department of Radiation Oncology, Massachusetts General Hospital, 149 13th Street, Charlestown, MA 02129, USA

Dmitriy N. Atochin [Prof.],
Cardiovascular Research Center, Department of Medicine, Massachusetts General Hospital, 149 13th Street, Charlestown, MA, 02129, United States of America

Hak Soo Choi [Prof.],

Gordon Center for Medical Imaging, Department of Radiology, Massachusetts General Hospital, 149 13th Street, Charlestown, MA 02129, USA

Satoshi Kashiwagi* **[Prof.]**
Gordon Center for Medical Imaging, Department of Radiology, Massachusetts General Hospital, 149 13th Street, Charlestown, MA 02129, USA

Abstract

Immunotherapy, including immune checkpoint inhibitors, has revolutionized cancer treatment, but only a minor fraction of patients shows durable responses. A new approach to overcome this limitation is yet to be identified. Recently, we have shown that photobiomodulation (PBM) with near-infrared (NIR) light in the NIR-II window reduces oxidative stress and supports the proliferation of $CD8^+$ T cells, suggesting that PBM with NIR-II light could augment anti-cancer immunity. Here we report a novel approach to support tumor-infiltrating $CD8^+$ T cells upon PBM with NIR-II laser with high tissue penetration depth. Brief treatments of a murine model of breast cancer with dual 1064 and 1270 nm lasers reduced expression of the programmed cell death protein 1 (PD-1) in $CD8^+$ T cells in a syngeneic mouse model of breast cancer. The direct effect of the NIR-II laser treatment on T cells was confirmed by the enhanced tumor growth delay by the adoptive transfer of laser-treated $CD8^+$ T cells *ex vivo* against a model tumor antigen. We further demonstrated that specific NIR-II laser parameters augmented the effect of the immune checkpoint inhibitor on tumor growth. PBM with NIR-II light augments the efficacy of cancer immunotherapy by supporting $CD8^+$ T cells. Unlike the current immunotherapy with risks of undesirable drug-drug interactions and severe adverse events, the laser is safe and low-cost. It can be broadly combined with other therapy without modification to achieve clinical significance. In addition, our study established a path to develop a novel laser-based therapy to treat cancer effectively.

Graphical Abstract

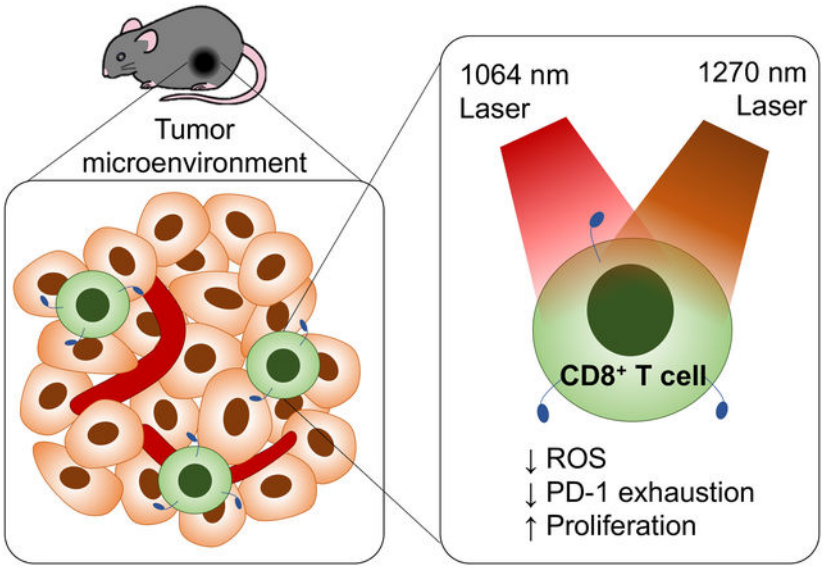

Photobiomodulation with 1064 and 1270 nm near-infrared laser in the NIR-II window reduces the expression of the programmed cell death receptor 1 (PD-1) in tumor-infiltrating $CD8^+$ T cells and enhances the effect of the immune checkpoint inhibitor on tumor progression in a mouse model of breast cancer, showing the potential of this approach to develop a novel laser-based immunotherapy for cancer.

Keywords

Immunotherapy; multispectral near-infrared II laser; T cell exhaustion; photobiomodulation; tumor microenvironment

1. Introduction

Monoclonal antibodies that block immune regulatory checkpoint receptors or their ligands have displayed remarkable effects and revolutionized the treatment of diverse cancers (1, 2). It is now believed that augmentation of anti-cancer immune responses would lead to the control of cancer and improve the long-term survival of cancer patients. However, tumor-specific adaptive responses can be inhibited by multiple immunosuppressive mechanisms within the tumor (1). As a result, only a minor fraction of cancer patients shows durable responses to the current immunotherapies (3). In addition, many tumor types are minimally responsive to this approach (3). To overcome this limitation, further efforts to improve the effects and breadth of immunotherapy through various multimodal approaches are underway. Human tumors are recognized by $CD4^+$ and $CD8^+$ T cells that target neoantigens (mutated proteins within the tumor) (4). The generation of neoantigen-specific T cells is a multistep system involving the processing and presentation of neoantigen by antigen-presenting cells (APCs) (5), which offers multiple opportunities for the tumor to escape immunosurveillance. Therefore, the development of immunotherapy that can reverse these immunosuppressive mechanisms is of considerable interest.

The adoptive transfer of *ex vivo* expanded autologous lymphocytes that specifically target proteins encoded by somatically mutated genes has induced durable responses and shown regressions in patients with the metastatic bile duct, colon, cervical, and breast cancers (6–11), which suggests that spontaneous responses are insufficient to clear established tumors and activation of tumor-specific T cells is the most critical step in immunotherapy. On the other hand, chimeric antigen receptor (CAR) T cell therapy, targeting CD19, successfully induced durable remissions of B cell leukemias and lymphomas (12, 13). In this approach, autologous T cells are isolated from the patient, genetically modified to express the CAR, which recognizes neoantigens independently of the major histocompatibility complex (MHC) presentation (13), and returned to the patient. These studies suggest that stimulation of neoantigen-specific T cells is a method to bypass the endogenous steps and augment anti-tumor immunity.

There are solid pieces of evidence for diverse biological effects of the treatment with low-power near-infrared (NIR) light in the NIR-I window between 630–900 nm, including analgesia, tissue regeneration, and reduction of inflammation (14–18), which are broadly defined as photobiomodulation (PBM) (16). Recently, we have demonstrated that NIR

laser between 1061–1301 nm in the NIR-II window (1000–1700 nm) also displays PBM by activating mitochondrial retrograde signaling (19–26), suggesting that a broader range of NIR light is useful for PBM. This discovery is significant for therapeutic intervention as NIR-II laser shows reduced scattering, minimal tissue absorption with high tissue penetration depth compared with NIR-I, and therefore suitable for therapeutic purposes (27–29). We have further demonstrated that dual NIR-II laser of 1064 and 1270 nm modulates calcium signaling and redox status of T cells *in vitro* via activation of mitochondrial cytochrome c oxidase (COX) at multiple absorption peaks (22). Since anti-oxidation has been established to confer T cells resistance to functional suppression in the immunosuppressive tumor microenvironment (TME) with excessive reactive oxygen species (ROS) (30), this laser-based technology could support T cell functions and anti-tumor immune response.

Here we report a new approach to support tumor-infiltrating T lymphocytes (TILs) with brief treatments of non-tissue damaging dual NIR-II laser. This laser-based, safe, and low-cost approach was shown to improve functions of TILs in a syngeneic mouse model of breast cancer. We have further demonstrated that the dual NIR-II laser treatment can enhance the effect of the immune checkpoint blockade suppressing tumor growth.

2 Material and Method

2.1. Animals

Eight-week-old female C57BL/6J (stock# 000664) and OT-I TCR-transgenic female B6.129S6-*Rag2*^{tm1Fwa} Tg(TcraTcrb)1100Mjb (stock# 2334-F) mice were purchased from Jackson Laboratories (USA) and Taconic Biosciences (USA), respectively. All mice were acclimated for at least two weeks at Massachusetts General Hospital (MGH). All animal procedures were approved by the Massachusetts General Hospital IACUC (protocol number 2009N000103) and performed under the Public Health Service Policy on Human Care of Laboratory Animals.

2.2. The design and assembly of a laser system

A continuous-wave (CW) Nd:YAG laser (λ = 1064 nm, Ventus, Laser Quantum, UK) and indium phosphide (InP) semiconductor diode laser (λ = 1270 nm, spectral width = 8 nm/3dB, 202–000, Veralase LLC, USA) were used as sources of NIR-II light. CW Indium gallium arsenide (InGaAs) semiconductor laser diodes (λ = 1064 or 1270 nm, LDX Optronics Inc., USA) were used as sources of NIR-II light for tissue damage study. The 1064 nm and 1270 nm laser beams were merged through a short-pass dichroic mirror (DMSP1200, Thorlabs, USA) and directed to a multimode optic fiber (Core = 200 μm, NA = 0.22, Thorlabs, USA) by an achromatic lens (AC127–025-C, Thorlabs, USA). The diverging laser was collimated by a plano-convex lens (LA1074-C, Thorlabs, USA). To obtain a homogenized flat-top intensity distribution of the beam, a holographic diffuser (47–680, Edmund Optics, USA) was used in the optical path. The beam diameter was then set to be 5 mm by adjusting the diameter of an aperture (Thorlabs, USA) and the distance between the iris and the irradiation plane of an animal (Supplementary Fig. S1). The optical system produced a circular target of 5 mm in diameter and 0.2 cm^2 in size, which was confirmed

by the infrared (IR) images of the spot as described previously (20). Different parameter settings are summarized in Table 1.

2.3. T Cell Harvesting

To obtain T cell culture, splenocytes were harvested from the mouse spleen. The spleen was mechanically disaggregated and passed through 70 μm and 40 μm mesh filters (Corning, USA). Then T cells were negatively selected from the splenocytes using magnetic beads (19851A, EasySep™ T cell isolation kit, STEMCELL Technologies, Canada). The purified T cells were suspended at a concentration of 1×10^6 cells/mL and incubated overnight in RPMI1640 (Thermo Fisher Scientific, USA) containing 10% fetal bovine serum (FBS, Thermo Fisher Scientific), 100 units/ml penicillin/streptomycin (Thermo Fisher Scientific), 0.1% 2-mercaptoethanol (Thermo Fisher Scientific) and 10 mM HEPES buffer (Thermo Fisher Scientific) in 37°C 5% CO_2 incubator.

2.4. T cell in vitro proliferation assay

To trace proliferation, isolated T cells were stained with carboxyfluorescein succinimidyl ester (CFSE, C34554, Thermo Fisher Scientific). Then the T cells were stimulated by magnetic beads covalently coupled to anti-CD3 and anti-CD28 antibodies (11453D, Thermo Fisher Scientific), and incubated in RPMI1640 containing 10% FBS, 100 units/ml penicillin/streptomycin, 0.1% 2-mercaptoethanol, 10 mM HEPES buffer, and 2.4 μg/mL Interleukin-2 (IL-2, 402-ML, R&D systems, USA). Flat clear bottom 96-well black plates (Corning) were used for the incubation and following laser treatment.

CW Nd:YAG laser (λ=1064 nm, 300 or 350 mW/cm^2) and diode laser (λ=1270 nm, 50 mW/cm^2) were used as illumination sources separately or simultaneously. The laser power was adjusted to obtain an indicated irradiance at the cell surface using a power meter. These laser lights were illuminated to the cells through the bottom of the well plate for 1 min. The parameters of the laser irradiance for *in vitro* studies were selected based on the previous report (22). The laser treatment was commenced daily for 4 consecutive days (4 times in total). At day 5, T cells were washed and labeled for CD3 (145–2C11, BioLegend, USA), CD4 (RM4–4, BioLegend), CD8 (53–6.7, eBioscience, USA), programmed cell death protein 1 (PD-1, 29F.1.A12, BioLegend) and Live/Dead Fixable Aqua (L34957, Life Technologies, USA). Data were acquired using a Fortessa flow cytometer (BD Bioscience, USA) and analyzed with FlowJo software version 10 (Flowjo Co. USA). Live T cells were identified by Live/Dead Aqua and CD3, and then the proliferation of $CD4^+$ and $CD8^+$ T cells was assessed by measuring CFSE dilution.

2.5. Measurement of intracellular ROS generation and mitochondrial activity in T cells

Isolated T cells were allocated into 96 well plates at 1×10^6 cells/well. CW Nd:YAG laser (λ=1064 nm, 150 or 300 mW/cm^2) and diode laser (λ=1270 nm, 50 or 100 mW/cm^2) lights were illuminated for 1 min followed by 2 h incubation at 37°C. The cells were then labeled for CD3, CD4, CD8 antibodies and CellROX Green (C10444, Invitrogen, USA), MitoSOX Red (M36008, Invitrogen) for 30 min. Flow cytometry analysis was performed immediately after the staining.

2.6. NIR-II laser treatment of T cells for adoptive transfer

$CD8^+$ T cells were isolated from OT-I TCR-transgenic mouse spleen as described in section 2.3. The source OT-I transgenic mice were obtained from Taconic Biosciences. Then the T cells were stimulated by magnetic beads covalently coupled to anti-CD3 and anti-CD28 antibodies after isolation and incubated in RPMI1640 containing 10% FBS, 100 units/ml penicillin/streptomycin, 0.1% 2-mercaptoethanol, 10 mM HEPES buffer, and 2.4 μg/mL IL-2 in the glass-bottom 96-well black plate. CW Nd:YAG laser (λ=1064 nm, 300mW/cm^2) and diode laser (λ=1270 nm, 50mW/cm^2) were simultaneously illuminated for 1 min for 5 consequent days. The parameters of the laser irradiance for in vitro studies were selected based on the previous report (22). Host C57BL/6J mice were obtained from Jackson Laboratory. The host mice were first subcutaneously injected with 2×10^6 murine medullary mammary adenocarcinoma (E0771) tumor cells (31–33) expressing ovalbumin (OVA) on day 1. For the E0771 cell line expressing OVA, E0771 cells were transduced with membrane-bound ovalbumin (Addgene 25099, USA) using a lentiviral vector that contains a mCherry reporter (AddGene 27362) as previously described elsewhere (34, 35). Cells with high mCherry expression were sorted out by flow cytometry and pooled. The isolated and *ex vivo* stimulated $CD8^+$ OT-I T cells (1×10^6 per mouse) were then injected retro-orbitally into mice on day 7. Transfer of equal numbers of no laser-treated OT-I T cells served as the control.

2.7. NIR-II laser treatment on breast cancer model

E0771 tumor cells syngeneic with C57BL/6 mice (31–33) were kept in RPMI1640 media with 10% FBS and 100 units/ml penicillin/streptomycin antibiotic cocktail. The cells were tested negative for adventitious mouse pathogens, including mycoplasma, at VRL Diagnostics (USA). For tumor injection, cells were harvested with 0.25% trypsin/EDTA (Thermo Fisher Scientific), centrifuged, re-suspended in sterile PBS, and kept on ice until injection. Congenic female C57BL/6J mice were used for E0771 tumor implantation at eight weeks of age. Animals were anesthetized with ketamine/xylazine (90/9 mg/kg), followed by implantation of 5×10^5 E0771 cells into the left and right flank skin using a 27-gauge needle. After the injection, caliper-measured tumor sizes were recorded at indicated time points in a blind manner for the observer.

Mouse hair was removed one day prior to tumor injection using a commercial depilatory cream (Nair, Church & Dwight Co., USA). 5×10^5 E0771 cells were injected into mice's left and right back sides subcutaneously on day 1. The tumors were then treated by dual NIR-II laser illumination with different parameters (1064 nm: 1.5–6 W/cm^2, 1270 nm: 0.25–1 W/cm^2, time: 30–120 s) for 5 consecutive days, from day 3 to 7, as shown in Supplementary Fig. S1. The laser power was adjusted to obtain an indicated irradiance at the skin surface using a power meter.

2.8. Combination treatment between dual NIR-II laser and immune checkpoint inhibitor in a breast cancer model

To determine the synergistic effect between dual NIR-II laser and immune checkpoint inhibitor treatment, 100 μg of anti-mouse PD-1-specific monoclonal antibody (clone RMP1–14, Bio X Cell, USA) or isotype control (clone 2A3, Bio X Cell) was intraperitoneally

injected on day 3 and 7 with or without laser treatment. The tumor volumes (length × width^2 × 0.5) were measured from day 7 to 39. For histology and flow cytometry studies, the laser was illuminated on both sides of the mouse tumors. The tumors were dissected on day 16, two weeks after the first laser treatment.

2.9. Histology study

To determine the impact of laser treatment on TILs, tumor tissues were fixed in 4% paraformaldehyde, dehydrated and paraffin-embedded, and sectioned at 3 μm thickness. Staining with hematoxylin and eosin (H&E) followed regular procedures. For immunohistochemistry of TILs and their phenotypic markers, primary antibodies against the following targets were used: CD4 (EPR19514, Abcam, UK), CD8 (4SM16, eBioscience, USA), and FOXP3 (FJK-16s, eBioscience). Sections were counterstained with hematoxylin.

To quantify TILs, slides were digitally scanned using Aperio GT2 (Leica Biosystems, Germany) at 40x magnification (0.253 μm/pixel resolution) to obtain brightfield images. The scanned whole-slide images were uploaded to the Aiforia image management and analysis platform (Aiforia Technologies, Finland) and then analyzed with a deep learning model developed with a deep convolutional neural network (CNN) and supervised learning. The CNN algorithm was trained to recognize cells from the digital images in Aiforia® Cloud. The algorithm was trained with 4 gigapixels of image data and a total of 5952 cells (4,818 cells for CD4 and CD8, 1,134 cells for FOXP3) to recognize TILs. The algorithm performance was validated against manual cell counts by one or two observers in 5 image regions that were not included in the training data. The tumor was divided into four areas: necrotic areas, peritumor, peripheral and central regions by hand. The necrotic areas were removed from the analysis.

2.10. Tissue damage study

To determine the adverse effect of exposures with dual NIR-II lasers, the depilated skin of anesthetized mice was exposed to various combinations of 1064 nm (1.5–6.0 W/cm^2) and 1270 nm (0.25–1.0 W/cm^2) NIR laser. Blood was drawn 24 h after the treatment and stained for May-Grunwald-Giemsa staining. Mice organs (skin, liver, kidney, bone marrow in the femur, spleen) were dissected and harvested with 4% paraformaldehyde. Five μm-thick paraffin sections were H&E-stained and examined for microscopic tissue damage and polymorphonuclear (PMN) infiltration.

Phototoxicity by exposures with dual NIR-II laser was also determined by immunoblot analysis (36). The depilated skin of anesthetized mice was exposed to various combinations of 1064 nm (1.5–6.0 W/cm^2) and 1270 nm (0.25–1.0 W/cm^2) NIR laser for 1 min. The treated skin was isolated 24 h after the completion of the laser exposure and lysed with RIPA lysis buffer (Thermo-Fisher Scientific) supplemented with cOmplete Protease Inhibitor Cocktail (Roche, Switzerland). The lysates were centrifuged, and the protein concentration was determined using a Pierce™ BCA Protein Assay Kit (Thermo-Fisher Scientific) using albumin as a standard. 20 μg of protein were suspended in a supplemented 4 × Laemmli Sample Buffer (Bio-Rad, USA) diluted in dH_2O (final concentration: 62.5 mM Tris-HCl, 10% glycerol, 0.0045% bromophenol blue, 1% LDS, and 355 mM 2-mercaptoethanol),

incubated for 10 min at 85°C. 25–40 μL of diluted samples and 10 μL of Precision Plus Protein™ Kaleidoscope™ Prestained Protein Standards (Bio-Rad, USA) were loaded in NOVEX WedgeWell 8–16% Tris-Glycine Gel 1.0 mm × 15 well (XP08165BOX, Invitrogen, USA). Resolved proteins were transferred to a polyvinylidene difluoride (PVDF) membrane (Millipore Immobilon-P Transfer membrane; Millipore Corp., USA). Following the transfer, the membranes were blocked with 5% bovine serum albumin (BSA) in Tris-buffered saline (TBS) with 1% Tween-20 (TBST) overnight at 4°C. Blocked membranes were then probed with the following primary antibodies for ATF-4 (ab1371, Abcam, USA), HSP70 (4872S, Cell Signaling Technology, USA), HSP90 (clone C45G5, 4877S, Cell Signaling); and GAPDH (clone 14C10, 2118L, Cell Signaling Technology) diluted with 1% BSA/TBST for 2 h at room temperature. Next, membranes were washed with TBST and incubated with the appropriate secondary antibody conjugated to horseradish peroxidase-conjugated anti-rabbit IgG (111–035-144 Jackson ImmunoResearch, USA) for 1 h at room temperature. Antibody binding was visualized using the Pierce™ ECL Western Blotting Substrate (Thermo Fisher Scientific) and imaged using the ChemiDoc MP imaging system (Bio-Rad). Densitometry data were quantified using Image J following established methods (37).

2.11. Flow Cytometry analysis

For the analysis of T cells in the tumor *in vivo*, dissected tumors were digested by freshly prepared collagenase I (1 mg/mL, 17100–017, Thermo Fisher Scientific), collagenase IV (250 U/mL, 17100–019, Thermo Fisher Scientific), DNase (100 U/mL, Sigma-Aldrich, USA) solution for 60 min. Dissociated cells were filtered through a 40 μm mesh and separated by Ficoll gradient media (17–1440-02, GE Healthcare, USA) to obtain TILs. The isolated cells were then labeled for CD3 (145–2C11, BioLegend), CD4 (RM4–4, BioLegend), CD8 (53–6.7, eBioscience), CD45 (30-F11, BioLegend), PD-1 (29F.1.A12, BioLegend), FOXP3 (MF23, BD Bioscience), Interferon-γ (IFN-γ, XMG1.2, BioLegend) and Live/Dead Fixable Aqua Dead cell stain kit (L34957, Invitrogen) to identify and characterize T cell subsets in tumors. The fluorescence data were acquired on a Fortessa flow cytometer and analyzed with FlowJo software ver. 10.

2.12. Statistical Analysis

One-way Analysis of Variance (ANOVA) followed by Tukey's multiple comparison tests was performed for flow cytometry analysis unless stated otherwise. Mixed model analysis with Geisser-Greenhouse correction or two-way ANOVA followed by Tukey's multiple comparison tests was performed for *in vivo* tumor growth analysis, and the Gehan-Breslow-Wilcoxon test was performed for the comparison of Kaplan-Meier survival curves. All the statistical analyses were carried out using GraphPad Prism version 8. The mean ± s.e.m. (the standard error of the mean) were displayed for all figures. An adjusted *P* value of less than 0.05 was regarded as statistically significant.

3 Results

3.1 Dual NIR-II laser treatment increased T cell proliferation in vitro

We have previously shown that dual NIR-II laser (1064 + 1270 nm) treatment shows PBM and temporally modulates intracellular calcium and ROS signaling in T cells *in vitro* (22),

which plays a critical role in regulating diverse T cell functions (38–42). Based on this data, we hypothesized that dual NIR-II laser treatment could have a long-term impact on the phenotype of T cells via modulation of calcium and ROS. To prove this hypothesis, we further determined the effect of dual NIR-II laser treatment on T cell proliferation and differentiation *in vitro*. Isolated T cells from the spleen were labeled with CFSE and stimulated by anti-CD3 and anti-CD28 antibodies. T cells were treated with either CW 1064 or 1270 nm only, or a mixture of 1064 nm (300 mW/cm^2) and 1270 nm (50 mW/cm^2) for 1 min per day for 4 consecutive days. On day 5, cell proliferation was analyzed by flow cytometry. As shown by representative flow cytometry gates (Fig. 1A), the levels of T-cell proliferation were assessed by percentages of CFSE-low cells among total CD4$^+$ or CD8$^+$ T cells (Fig. 1B). Percentages of CFSE-low cells with more than three proliferation cycles among CD4$^+$ T cells were not significantly changed with any laser treatment (Fig. 1C). Interestingly, while the percentages of proliferating CD8$^+$ T cells treated with the laser of a single wavelength were marginally increased, those treated with dual NIR-II laser were significantly increased (Fig. 1D, $P = 0.0048$). Laser treatment did not induce any notable change in the CD4/CD8 T cell ratio (Fig. 1E). Consistent with our previous study (22), this dose of dual NIR-II laser reduced cytosolic ROS generation in CD4$^+$ (Fig. 2A, $P = 0.0429$) and CD8$^+$ T cells (Fig. 2B, $P = 0.0429$) in the acute phase. These results suggest that sustained reduction of ROS improved T cell function. The dual NIR-II laser did not significantly affect the expression of the exhaustion marker PD-1 in CD8$^+$ T cells (Supplementary Fig. S2A). At the same time, it induced a statistically marginal increase in the expression of the activation marker CD69 (Supplementary Fig. S2B). In our previous study (22), we identified multiple absorption peaks of a putative photoreceptor COX in the NIR-II region. Together, these results suggest that dual NIR-II laser treatment has the potential to show a superior effect to single NIR-II laser treatment in modulating T cell function and inducing T cell proliferation.

3.2 Dual laser treatment modestly suppressed tumor growth in vivo

Cancer is known to produce high amounts of ROS, which modulate the immune function of T cells (43). A recent study has shown that central memory T cells with higher antioxidant levels survive longer in a tumor and are able to suppress tumor growth (30). Based on our previous result that dual NIR-II laser treatment modulated ROS signaling (22), we hypothesized that treatment of solid tumors with dual laser treatment could improve the function of TILs and augment anti-tumor immunity. To test this hypothesis, we determined the impact of dual NIR-II laser treatment on tumor growth in a mouse model of breast cancer.

First, we determined if dual NIR-II laser exposures show any adverse effects. The depilated skin was exposed to various combinations of 1064 nm (1.5–6.0 W/cm^2) and 1270 nm (0.25–1.0 W/cm^2) dual NIR-II laser. Non-tissue damaging combinations were determined to be those at which skin temperatures did not exceed 43°C and for which no visible or microscopic damage or changes were detected (20). We identified a combination of 1064 nm up to 3 W/cm^2 and 1270 nm up to 1 W/cm^2 as the maximum safe irradiance for one minute (Fig. 3A). Since phototoxicity by exposures to NIR laser could be mediated by heat or ROS, we next determined tissue damage markers by immunoblot analysis as established elsewhere

(36). The depilated skin was exposed to various combinations of NIR laser, isolated 24 h after the completion of the laser exposure, and analyzed. Levels of activating transcription factor-4 (ATF-4), heat shock protein 90 (HSP90), and HSP70, which are established markers for tissue damage, were determined by immunoblot analysis. The non-invasive doses used in this study did not induce appreciable change in the expression of ATF-4, HSP90, or HSP70 (Fig. 3B). Consistently with the published study (36), the tissue-damaging dose of dual NIR-II laser with 1064 nm at 6.0 W/cm^2 and 1270 nm at 1.0 W/cm^2 decreased HSP70 and ATF-4 expression due to extensive tissue damage (Fig. 3B). With these combinations of non-tissue damaging doses, neither tissue damage nor inflammatory response was detected in the treated skin, blood, and other major vital organs (Supplementary Fig. S3).

We next determined the impact of dual NIR-II laser treatment on tumor growth in the E0771 syngeneic mouse model of breast cancer. In order to assess the involvement of the immune system, tumors were established on both sides of the flank skin, but only the tumors on the right side were treated with lasers. The tumors were treated with various combinations of 1064 nm (1.5–6.0 W/cm^2) and 1270 nm (0.25–1.0 W/cm^2) for 30–120 s for 5 consecutive days to seek an optimal dose for *in vivo* applications (Supplementary Fig. 4A). Any treatment resulted in modest tumor growth delay on both treated and non-treated sides of the tumor (Supplementary Fig. 4B). Noteworthy, some of the parameters slightly suppressed tumor growth (Supplementary Fig. 4B–C). Mice treated with the dual NIR-II laser did not prolong the time to a defined clinical endpoint (Supplementary Fig. 4D). Together, these results indicate that the dual NIR-II laser treatment alone has little impact on tumor growth.

3.3 Dual NIR-II laser treatment decreased the expression of PD-1 on CD8$^+$ T cells

We next determine the effect of the dual NIR-II laser on T cells in tumor tissue. We isolated TILs treated by the NIR-II laser and analyzed their subpopulations and effector functions by flow cytometry (Fig. 4A). In this study, we treated tumors with various combinations of 1064 nm and 1270 nm, as established above. Laser treatment did not affect FOXP3 positive regulatory T cell (Treg) subpopulations to CD4$^+$ T cells, which play a critical role in suppressing anti-tumor immune responses (Fig. 4B). Intriguingly, specific combinations of dual NIR-II laser treatment led to a decrease in exhausted PD-1$^+$ CD8$^+$ T cells compared to non-treated tumors (Fig. 4C). In particular, the dual NIR-II laser treatment with 1064 nm at 3 W/cm^2 combined with 1270 nm at 1 W/cm^2 for 1 min induced a marginal decrease in PD-1$^+$ CD8$^+$ T cells compared to the no laser control (Fig. 4C, $P = 0.0663$). Importantly, a smaller dose of the dual NIR-II laser treatment with 1064 nm at 1.5 W/cm^2 combined with 1270 nm at 0.25 W/cm^2 for 1 min induced a significant decrease in PD-1$^+$ CD8$^+$ T cells (Fig. 4C, $P = 0.0354$). However, these effects did not lead to improved effector function of CD8$^+$ T cells with no apparent changes in IFN-γ expression levels (Fig. 4D) or granzyme B levels (data not shown). These results indicate that dual NIR-II laser treatment modulates the functions of TILs *in vivo*.

To determine the impact of dual laser treatment, we evaluated CD4$^+$, FOXP3$^+$, and CD8$^+$ T cells by immunohistochemistry (Supplementary Fig. S5). For quantitation of TILs, the tumor was divided into three areas: peritumor, peripheral and central regions

(Supplementary Fig. S5A) (44, 45). The necrotic areas were removed from the analysis (44, 45). Combinations of 1064 nm and 1270 nm had minor effects on $CD4^+$and $FOXP3^+$ cells in peritumor (Supplementary Fig. S5B) and central (Supplementary Fig. S5D) areas. In contrast, the specific combinations of 1064 nm and 1270 nm (1064 nm 3 or 1.5 W/cm^2 + 1270 nm 1 or 0.25 W/cm^2 for 1 min), which decreased PD-1^+ $CD8^+$ T cells (Fig. 4C), also showed a marginal increase in $CD8^+$ T cells in peripheral (Supplementary Fig. S5C) and central (Supplementary Fig. S5D) areas compared to the non-treated tumor, which is consistent with the *in vitro* data showing its positive effect on $CD8^+$ T cell proliferation and negative impact on PD-1 expression. Together, these results implicate that only specific combinations of laser parameters, namely 1064 nm 3 or 1.5 W/cm^2 + 1270 nm 1 or 0.25 W/cm^2 for 1 min, could support augmentation of anti-tumor immunity.

3.4 Dual NIR-II laser treatment enhanced the efficacy of adoptive transfer therapy

Although the dual NIR-II laser treatment was able to modulate T cell function *in vitro* and *in vivo*, it induced only modest suppression of tumor growth in a mouse model of breast cancer (Supplementary Fig. S4). These observations suggest that the dual NIR laser treatment could improve the effector function of T cells, but it may not be sufficient to overcome the immunosuppressive TME. To test this hypothesis, we next performed adoptive T cell transfer (46–48). In this system, if direct laser treatment of isolated T cells *ex vivo* still shows positive effects, the effect of dual NIR laser on T cells is proven to mediate the beneficial effect of dual NIR-II laser on tumor progression. In addition, such an observation would further indicate that the immunosuppressive TME diminishes the effect of dual NIR-II laser treatment. To this end, we also used E0771 cells, which were engineered to express OVA as a model tumor antigen (Fig. 5A). Transfer of $CD8^+$ OT-I T cells treated with no laser provided no benefit in suppressing tumor growth over no adoptive transfer control (Fig. 5B–C), suggesting that $CD8^+$ OT-I T cells have little impact on tumor growth without proper support mechanisms in this model. On the other hand, the transfer of $CD8^+$ OT-I T cells treated with dual laser treatment significantly suppressed tumor growth compared to the transfer of untreated $CD8^+$ OT-I T cells (Fig. 5B–C, $P = 0.0245$ at day 39) or no transfer ($P = 0.0248$). Consistently, mice that were adoptively transferred with laser-treated $CD8^+$ OT-I T cells survived longer than those that received untreated $CD8^+$ OT-I T cells (Fig. 5D, $P = 0.0358$) or untreated cells ($P = 0.0135$). These data indicate that dual NIR-II laser treatment has direct effects on $CD8^+$ T cell functions and is able to contribute to the suppression of tumor growth *in vivo*.

3.5 Dual NIR-II laser treatment enhanced the efficacy of the immune checkpoint blockade on tumor growth

Since our data suggest that dual NIR-II laser treatment modulates PD-1 expression on $CD8^+$ T cells, which is established to inhibit T-cell receptor signaling, proliferation, and activity and induce adaptive immune resistance (49, 50), the laser treatment could further augment the effect of immunotherapy with anti-PD-1 or anti-PD-L1 antibody to reactivate cytotoxic T cells. To test this hypothesis, we determined the therapeutic efficacy of combination therapy of the dual NIR-II laser treatment with anti-PD-1 antibody. Tumors were established on both sides of the flank skin, and then tumors on the one side were treated with the dual NIR-II laser for 5 consecutive days and anti-PD-1 antibody at the beginning and end of the laser

treatment (twice in total). Two effective parameters in the TIL study *in vivo* (1064 nm at 3 W/cm^2 and 1270 nm at 1 W/cm^2 for 1 min, 1064 nm at 1.5 W/cm^2, and 1270 nm at 0.25 W/cm^2 for 1 min) were selected for this study (Fig. 6A). As expected, anti-PD-1 and dual NIR-II laser treatment alone showed modest effects on tumor growth on both laser-treated and non-laser-treated tumors (Fig. 6B). The combination therapy showed significant tumor growth delay on the laser-treated side of tumors compared to no therapy or anti-PD-1 antibody treatment alone (Fig. 6B, no laser vs. 1064 nm at 3 W/cm^2 and 1270 nm at 1 W/cm^2 + αPD-1: $P = 0.0403$, PD-1 vs. 1064 nm at 1.5 W/cm^2 and 1270 nm at 0.25 W/cm^2 + αPD-1: $P = 0.0020$ at day 33) and a significant prolongation of survival of tumor-bearing mice (Fig. 6C, no laser vs. 1064 nm at 3 W/cm^2 and 1270 nm at 1 W/cm^2 + αPD-1: $P = 0.0315$). These results suggest that the NIR-II laser treatment synergistically suppressed tumor growth when combined with the immune checkpoint blockade.

3.6 Dual NIR-II laser treatment enhanced the efficacy of the immune checkpoint blockade on CD8$^+$ T cells

We next determined the effect of the combination therapy on T cells in the TME. To this end, we isolated TILs from tumors treated with the NIR-II laser and analyzed their subpopulations and effector functions by flow cytometry. The combination therapy did not affect FOXP3$^+$ regulatory T cells (Fig. 7A). Specific combinations of the dual NIR-II laser treatment with the immune checkpoint inhibitor led to a decrease in exhausted PD-1$^+$ CD8$^+$ T cells compared to no therapy or anti-PD-1 or dual NIR-II laser treatment alone (Fig. 7B). In particular, anti-PD-1 treatment combined with the dual NIR-II laser treatment with 1064 nm at 1.5 W/cm^2 and 1270 nm at 0.25 W/cm^2 for 1 min induced a significant decrease in PD-1^{high} CD8$^+$ T cells as compared to the no laser control (Fig. 7B, $P = 0.0087$) or control IgG treatment only ($P = 0.0488$). However, these effects led to minor changes in IFN-γ expression levels in CD8$^+$ T cells (Figure 7C) or PD-1 or IFN-γ expression levels in CD4$^+$ T cells (Supplementary Fig. S7). These results support evidence of synergy between the dual NIR-II laser treatment and immune checkpoint blockade on CD8$^+$ T cell function.

4 Discussion

In the current study, we have, for the first time, established a laser-based technology to support TILs using a specific combination of NIR laser wavelengths in the NIR-II window. We have also demonstrated the efficacy of the dual NIR-II laser in augmenting the effect of cancer immunotherapy when combined with an immune checkpoint inhibitor in a mouse model of breast cancer. The impact of the NIR-II laser treatment on CD8$^+$ T cells was further validated by the enhanced tumor growth delay with the adoptive transfer of *ex vivo* laser-treated CD8$^+$ T cells against a model cancer antigen. It has been well established that anti-tumor T-cell responses can control tumors (51). The use of an immune checkpoint inhibitor or adoptive cellular transfer may be able to overcome the immunosuppression of T cells in the TME. Our data have clearly shown that the dual NIR-II laser treatment is one way to overcome the immunosuppressive effects of the TME, decreasing PD-1 expression of CD8$^+$ T cells and augmenting anti-cancer immune responses. Importantly, our approach does not require any additional agents to achieve this goal. Unlike most of the current immunotherapy with risks of undesirable drug-drug interactions, which could limit

the choice of therapy and negatively impact the efficacy and safety of therapy, the laser can be broadly combined with other therapeutics without modification to achieve clinical significance. Thus, the laser-based approach can be broadly combined with other modalities and could be used to further improve the efficacy of the current and candidate cancer therapies.

Interestingly, we have found that specific combinations of 1064 and 1270 nm were effective. In our previous study, we have shown that a putative photoreceptor for NIR light, COX, in mitochondria could absorb multiple wavelengths of NIR-II light, which would result in the release of nitric oxide (NO) (22). Each absorption would have distinct effects and promote or inhibit a particular function of the molecule. Modulation of interactions between COX and NO in mitochondria has been linked to the modulation of mitochondrial ROS generation (52, 53). NIR light in the NIR-I window has been shown to alter cell metabolism by mitochondrial ROS generation via modulating interactions between COX and NO (54–57). We further demonstrated that a combination of 1064 and 1270 nm laser in the NIR-II window modulated mitochondrial retrograde signaling, including intracellular calcium and ROS (22). However, the use of this signaling for therapy needs close attention to a selection of laser parameters that will be applied. For example, brief exposure of the skin of human subjects with 1064 nm NIR light at an irradiance of 250 mW/cm^2 has been reported to improve COX and hemoglobin oxygenation (58). In contrast, COX activity has been suppressed by dual laser treatment with 750 and 950 nm lasers (59, 60). In the current study, the treatment with the dual NIR-II of 1064 nm at 1.5 W/cm^2 and 1270 nm at 0.25 W/cm^2 for 1 min decreased PD-1 expression in $CD8^+$ T cells, while the treatment with the same wavelengths at the same power density for 2 min did not show such an effect (Fig. 4). Although the details on molecular mechanisms and pathways for the reduction remain elusive and need to be defined, these results suggest that an optimal combination of NIR light parameters can be identified for the desired outcome. Further investigation is warranted to explore such a combination of wavelength, irradiance, pulse width, and treatment time of this laser technology to effectively suppress the tumor growth of a particular type of tumor.

In the current study, the optimized dual CW NIR-II treatment led to a slight improvement in the effector function of $CD8^+$ T cells. At the same time, it was able to suppress the expression of PD-1 *in vivo* (Fig. 4, 7, Supplementary Fig. S7) and tumor growth when combined with an immune checkpoint inhibitor (Fig. 6, Supplementary Fig. S6). ROS are known to modulate the differentiation and effector functions of T cells. High environmental ROS lead to the development of T helper (T_H) 2 cells with increased IL-2 and IL-4 production, which is not favorable for shaping anti-cancer responses (61, 62). In contrast, a low level of ROS may promote T_H1 and T_H17 cell differentiation, and the use of antioxidants has been reported to increase IFN-γ production and skew the immune response to a T_H1 phenotype, which would be favorable for anti-cancer responses (61, 63, 64). Cancer is known to produce high amounts of ROS and modulate the immune function of T cells (43). Thus, cellular antioxidant levels are critical for the anti-tumor function of T cells in the TME. A recent study demonstrated that central memory T cells with higher cytosolic glutathione, surface thiol, and intracellular antioxidant levels survive longer in the TME to control tumor growth than effector memory T cells with less antioxidant levels and that antioxidant treatment improved the function of TILs and prolonged survival

of cancer patients (30). TILs are known to kill multiple cancer cells once they enter the TME (65, 66). These results indicate that longevity of TILs is critical to controlling tumor growth. Although our approach *per se* did not improve effector function, it contributed to the longevity of TILs in the TME and an increase of cell killing activity per $CD8^+$ T cells. Further investigation is warranted to determine the longevity of T cells in the TME and measure tumor cell killing per $CD8^+$ T cells upon the treatment using an optimized combination of NIR-II laser parameters in the future.

The NIR-II light-based immunotherapy has numerous advantages as a therapeutic intervention, including deep penetration into tissues (29) and the absence of carcinogenic or mutagenic properties (67). With the correct settings, the NIR laser poses little or no risk of side effects (Fig. 3, Supplementary Fig. S3). The laser-based approach is safe, effective, low-cost, and can be combined with not only other modalities of cancer immunotherapy toward the eradication of cancer but also other therapies for autoimmune diseases, allergies, and infectious diseases to augment further the therapeutic efficacy beyond cancer therapy.

5 Conclusion

In the current study, we have demonstrated that 1 min exposure of solid tumor and *ex vivo* $CD8^+$ T cell with a specific combination of 1064 nm and 1270 nm NIR lasers in the NIR-II window at low irradiances improves $CD8^+$ T cell functions and suppresses tumor growth when being combined with another immunotherapy. These results indicate that a parameter of NIR light beyond 1000 nm can be used to augment the efficacy of cancer immunotherapy. This study provides a rationale for the clinical combination of the dual NIR-II laser therapy and immune checkpoint blockade.

Supplementary Material

Refer to Web version on PubMed Central for supplementary material.

Acknowledgments:

This work was supported by TERUMO Co. (S.K.), Grant-in-Aid to the Program for Leading Graduate School for “Science for Development of Super Mature Society” from the Ministry of Education, Culture, Sport, Science and Technology in Japan (W.K.), the Research Grant of Keio Leading-edge Laboratory of Science and Technology (W.K.), Japan Society for the Promotion of Science Overseas Challenge Program for Young Researchers (W.K.), Global Scholarship of the Japan Business Federation (W.K.), a study abroad scholarship of CMI Inc., Tokyo, Japan (S.Y.), Deutsche Forschungsgemeinschaft (DFG, German Research Foundation) – Projektnummer 335549539 – GRK 2381 (S.F.), the Reinhard Frank-Stiftung (S.F.), the National Institute of Allergy and Infectious Diseases of the National Institutes of Health under award number R01AI105131 (S.K.), R21AI144103 (S.K.) and the National Institute of Neurological Disorders and Stroke R01NS096237 (D.N.A.), and Massachusetts General Hospital Executive Committee On Research (ECOR) Interim Support Funding (S.K.).

Data Availability Statements:

The data that support the findings of this study are available on request from the corresponding author. The data are not publicly available due to privacy or ethical restrictions.

Non-standard abbreviations:

APC	antigen-presenting cell
ATF-4	activating transription factor 4
BSA	bovine serum albumin
CAR	chimeric antigen receptor
CFSE	carboxyfluorescein succinimidyl ester
CNN	convolutional neural network
COX	cytochrome c oxidase
CW	continuous-wave
FBS	fetal bovine serum
H&E	hematoxylin and eosin
HSP	heat shock protein
IFN-γ	interferon-γ
IL-2	interleukin-2
InGaAs	indium gallium arsenide
InP	indium phosphide
IR	infrared
MHC	major histocompatibility complex
NIR	near-infrared
NO	nitric oxide
OVA	ovalbumin
PBM	photobiomodulation
PD-1	programmed cell death protein 1
PMN	polymorphonuclear
PVDF	polyvinylidene difluoride
ROS	reactive oxygen species
TBS	Tris-buffered saline
T_H1	T helper cell type 1
TIL	tumor-infiltrating T lymphocyte

TME	tumor microenvironment
Treg	regulatory T cell

References

1. Wilkinson RW, and Leishman AJ (2018) Further Advances in Cancer Immunotherapy: Going Beyond Checkpoint Blockade. Front Immunol 9, 1082 [PubMed: 29910800]
2. Topalian SL, Drake CG, and Pardoll DM (2015) Immune checkpoint blockade: a common denominator approach to cancer therapy. Cancer Cell 27, 450–461 [PubMed: 25858804]
3. Mellman I, Hubbard-Lucey VM, Tontonoz MJ, Kalos MD, Chen DS, Allison JP, Drake CG, Levitsky H, Lonberg N, van der Burg SH, Fearon DT, Wherry EJ, Lowy I, Vonderheide RH, and Hwu P (2016) De-Risking Immunotherapy: Report of a Consensus Workshop of the Cancer Immunotherapy Consortium of the Cancer Research Institute. Cancer Immunol Res 4, 279–288 [PubMed: 27036972]
4. Tran E, Robbins PF, and Rosenberg SA (2017) 'Final common pathway' of human cancer immunotherapy: targeting random somatic mutations. Nat Immunol 18, 255–262 [PubMed: 28198830]
5. Sade-Feldman M, Jiao YJ, Chen JH, Rooney MS, Barzily-Rokni M, Eliane JP, Bjorgaard SL, Hammond MR, Vitzthum H, Blackmon SM, Frederick DT, Hazar-Rethinam M, Nadres BA, Van Seventer EE, Shukla SA, Yizhak K, Ray JP, Rosebrock D, Livitz D, Adalsteinsson V, Getz G, Duncan LM, Li B, Corcoran RB, Lawrence DP, Stemmer-Rachamimov A, Boland GM, Landau DA, Flaherty KT, Sullivan RJ, and Hacohen N (2017) Resistance to checkpoint blockade therapy through inactivation of antigen presentation. Nature communications 8, 1136
6. Tran E, Ahmadzadeh M, Lu YC, Gros A, Turcotte S, Robbins PF, Gartner JJ, Zheng Z, Li YF, Ray S, Wunderlich JR, Somerville RP, and Rosenberg SA (2015) Immunogenicity of somatic mutations in human gastrointestinal cancers. Science 350, 1387–1390 [PubMed: 26516200]
7. Tran E, Turcotte S, Gros A, Robbins PF, Lu YC, Dudley ME, Wunderlich JR, Somerville RP, Hogan K, Hinrichs CS, Parkhurst MR, Yang JC, and Rosenberg SA (2014) Cancer immunotherapy based on mutation-specific CD4+ T cells in a patient with epithelial cancer. Science 344, 641–645 [PubMed: 24812403]
8. Tran E, Robbins PF, Lu YC, Prickett TD, Gartner JJ, Jia L, Pasetto A, Zheng Z, Ray S, Groh EM, Kriley IR, and Rosenberg SA (2016) T-Cell Transfer Therapy Targeting Mutant KRAS in Cancer. N Engl J Med 375, 2255–2262 [PubMed: 27959684]
9. Zacharakis N, Chinnasamy H, Black M, Xu H, Lu YC, Zheng Z, Pasetto A, Langhan M, Shelton T, Prickett T, Gartner J, Jia L, Trebska-McGowan K, Somerville RP, Robbins PF, Rosenberg SA, Goff SL, and Feldman SA (2018) Immune recognition of somatic mutations leading to complete durable regression in metastatic breast cancer. Nat Med 24, 724–730 [PubMed: 29867227]
10. Stevanovic S, Pasetto A, Helman SR, Gartner JJ, Prickett TD, Howie B, Robins HS, Robbins PF, Klebanoff CA, Rosenberg SA, and Hinrichs CS (2017) Landscape of immunogenic tumor antigens in successful immunotherapy of virally induced epithelial cancer. Science 356, 200–205 [PubMed: 28408606]
11. Goff SL, Dudley ME, Citrin DE, Somerville RP, Wunderlich JR, Danforth DN, Zlott DA, Yang JC, Sherry RM, Kammula US, Klebanoff CA, Hughes MS, Restifo NP, Langhan MM, Shelton TE, Lu L, Kwong ML, Ilyas S, Klemen ND, Payabyab EC, Morton KE, Toomey MA, Steinberg SM, White DE, and Rosenberg SA (2016) Randomized, Prospective Evaluation Comparing Intensity of Lymphodepletion Before Adoptive Transfer of Tumor-Infiltrating Lymphocytes for Patients With Metastatic Melanoma. J Clin Oncol 34, 2389–2397 [PubMed: 27217459]
12. Park JH, Riviere I, Gonen M, Wang X, Senechal B, Curran KJ, Sauter C, Wang Y, Santomasso B, Mead E, Roshal M, Maslak P, Davila M, Brentjens RJ, and Sadelain M (2018) Long-Term Follow-up of CD19 CAR Therapy in Acute Lymphoblastic Leukemia. N Engl J Med 378, 449–459 [PubMed: 29385376]
13. Brown CE, Alizadeh D, Starr R, Weng L, Wagner JR, Naranjo A, Ostberg JR, Blanchard MS, Kilpatrick J, Simpson J, Kurien A, Priceman SJ, Wang X, Harshbarger TL, D'Apuzzo M, Ressler JA, Jensen MC, Barish ME, Chen M, Portnow J, Forman SJ, and Badie B (2016) Regression of

Glioblastoma after Chimeric Antigen Receptor T-Cell Therapy. N Engl J Med 375, 2561–2569 [PubMed: 28029927]

14. Huang YY, Chen AC, Carroll JD, and Hamblin MR (2009) Biphasic dose response in low level light therapy. Dose Response 7, 358–383 [PubMed: 20011653]
15. Huang YY, Sharma SK, Carroll J, and Hamblin MR (2011) Biphasic dose response in low level light therapy - an update. Dose Response 9, 602–618 [PubMed: 22461763]
16. Karu T (2013) Is it time to consider photobiomodulation as a drug equivalent? Photomed Laser Surg 31, 189–191 [PubMed: 23600376]
17. Karu T (2010) Mitochondrial mechanisms of photobiomodulation in context of new data about multiple roles of ATP. Photomed Laser Surg 28, 159–160 [PubMed: 20374017]
18. Karu TI (2010) Multiple roles of cytochrome c oxidase in mammalian cells under action of red and IR-A radiation. IUBMB life 62, 607–610 [PubMed: 20681024]
19. Kashiwagi S, Yuan J, Forbes B, Hibert ML, Lee EL, Whicher L, Goudie C, Yang Y, Chen T, Edelblute B, Collette B, Edington L, Trussler J, Nezivar J, Leblanc P, Bronson R, Tsukada K, Suematsu M, Dover J, Brauns T, Gelfand J, and Poznansky MC (2013) Near-infrared laser adjuvant for influenza vaccine. PLoS One 8, e82899 [PubMed: 24349390]
20. Kimizuka Y, Callahan JJ, Huang Z, Morse K, Katagiri W, Shigeta A, Bronson R, Takeuchi S, Shimaoka Y, Chan MP, Zeng Y, Li B, Chen H, Tan RY, Dwyer C, Mulley T, Leblanc P, Goudie C, Gelfand J, Tsukada K, Brauns T, Poznansky MC, Bean D, and Kashiwagi S (2017) Semiconductor diode laser device adjuvanting intradermal vaccine. Vaccine 35, 2404–2412 [PubMed: 28365253]
21. Kimizuka Y, Katagiri W, Locascio JJ, Shigeta A, Sasaki Y, Shibata M, Morse K, Sirbulescu RF, Miyatake M, Reeves P, Suematsu M, Gelfand J, Brauns T, Poznansky MC, Tsukada K, and Kashiwagi S (2018) Brief Exposure of Skin to Near-Infrared Laser Modulates Mast Cell Function and Augments the Immune Response. J Immunol 201, 3587–3603 [PubMed: 30420435]
22. Katagiri W, Lee G, Tanushi A, Tsukada K, Choi HS, and Kashiwagi S (2020) High-throughput single-cell live imaging of photobiomodulation with multispectral near-infrared lasers in cultured T cells. J Biomed Opt 25, 1–18
23. Kashiwagi S (2020) Laser adjuvant for vaccination. FASEB J 34, 3485–3500 [PubMed: 31994227]
24. Kashiwagi S, Brauns T, Gelfand J, and Poznansky MC (2014) Laser vaccine adjuvants. History, progress, and potential. Hum Vaccin Immunother 10, 1892–1907 [PubMed: 25424797]
25. Kashiwagi S, Brauns T, and Poznansky MC (2016) Classification of Laser Vaccine Adjuvants. J Vaccines Vaccin 7, 307 [PubMed: 27104047]
26. Morse K, Kimizuka Y, Chan MPK, Shibata M, Shimaoka Y, Takeuchi S, Forbes B, Nirschl C, Li B, Zeng Y, Bronson RT, Katagiri W, Shigeta A, Sirbulescu RF, Chen H, Tan RYY, Tsukada K, Brauns T, Gelfand J, Sluder A, Locascio JJ, Poznansky MC, Anandasabapathy N, and Kashiwagi S (2017) Near-Infrared 1064 nm Laser Modulates Migratory Dendritic Cells To Augment the Immune Response to Intradermal Influenza Vaccine. J Immunol 199, 1319–1332 [PubMed: 28710250]
27. Lee JH, Park G, Hong GH, Choi J, and Choi HS (2012) Design considerations for targeted optical contrast agents. Quant Imaging Med Surg 2, 266–273 [PubMed: 23289086]
28. Hu S, Kang H, Baek Y, El Fakhri G, Kuang A, and Choi HS (2018) Real-Time Imaging of Brain Tumor for Image-Guided Surgery. Advanced healthcare materials, e1800066
29. Owens EA, Henary M, El Fakhri G, and Choi HS (2016) Tissue-specific near-infrared fluorescence imaging. Accounts of chemical research 49, 1731–1740 [PubMed: 27564418]
30. Scheffel MJ, Scurti G, Simms P, Garrett-Mayer E, Mehrotra S, Nishimura MI, and Voelkel-Johnson C (2016) Efficacy of Adoptive T-cell Therapy Is Improved by Treatment with the Antioxidant N-Acetyl Cysteine, Which Limits Activation-Induced T-cell Death. Cancer Res 76, 6006–6016 [PubMed: 27742673]
31. Gomes-Santos IL, Amoozgar Z, Kumar AS, Ho WW, Roh K, Talele NP, Curtis H, Kawaguchi K, Jain RK, and Fukumura D (2021) Exercise training improves tumor control by increasing CD8+ T-cell infiltration via CXCR3 signaling and sensitizes breast cancer to immune checkpoint blockade. Cancer Immunol Res
32. Ager EI, Kozin SV, Kirkpatrick ND, Seano G, Kodack DP, Askoxylakis V, Huang Y, Goel S, Snuderl M, Muzikansky A, Finkelstein DM, Dransfield DT, Devy L, Boucher Y, Fukumura D,

and Jain RK (2015) Blockade of MMP14 activity in murine breast carcinomas: implications for macrophages, vessels, and radiotherapy. J Natl Cancer Inst 107: djv017.

33. Incio J, Ligibel JA, McManus DT, Suboj P, Jung K, Kawaguchi K, Pinter M, Babykutty S, Chin SM, Vardam TD, Huang Y, Rahbari NN, Roberge S, Wang D, Gomes-Santos IL, Puchner SB, Schlett CL, Hoffmman U, Ancukiewicz M, Tolaney SM, Krop IE, Duda DG, Boucher Y, Fukumura D, and Jain RK (2018) Obesity promotes resistance to anti-VEGF therapy in breast cancer by up-regulating IL-6 and potentially FGF-2. Sci Transl Med 10: eaag0945.
34. Yang J, Sanderson NS, Wawrowsky K, Puntel M, Castro MG, and Lowenstein PR (2010) Kupfer-type immunological synapse characteristics do not predict anti-brain tumor cytolytic T-cell function in vivo. Proc Natl Acad Sci U S A 107, 4716–4721 [PubMed: 20133734]
35. Weber K, Bartsch U, Stocking C, and Fehse B (2008) A multicolor panel of novel lentiviral "gene ontology" (LeGO) vectors for functional gene analysis. Mol Ther 16, 698–706 [PubMed: 18362927]
36. Khan I, Tang E, and Arany P (2015) Molecular pathway of near-infrared laser phototoxicity involves ATF-4 orchestrated ER stress. Scientific reports 5, 10581
37. Stael S, Miller LP, Fernandez-Fernandez AD, and Van Breusegem F (2022) Detection of Damage-Activated Metacaspase Activity by Western Blot in Plants. Methods Mol Biol 2447, 127–137 [PubMed: 35583778]
38. Kaminski MM, Sauer SW, Kaminski M, Opp S, Ruppert T, Grigaravicius P, Grudnik P, Grone HJ, Krammer PH, and Gulow K (2012) T cell activation is driven by an ADP-dependent glucokinase linking enhanced glycolysis with mitochondrial reactive oxygen species generation. Cell reports 2, 1300–1315 [PubMed: 23168256]
39. Feske S, Wulff H, and Skolnik EY (2015) Ion channels in innate and adaptive immunity. Annu Rev Immunol 33, 291–353 [PubMed: 25861976]
40. Sena LA, Li S, Jairaman A, Prakriya M, Ezponda T, Hildeman DA, Wang CR, Schumacker PT, Licht JD, Perlman H, Bryce PJ, and Chandel NS (2013) Mitochondria are required for antigen-specific T cell activation through reactive oxygen species signaling. Immunity 38, 225–236 [PubMed: 23415911]
41. Trebak M, and Kinet JP (2019) Calcium signalling in T cells. Nat Rev Immunol 19, 154–169 [PubMed: 30622345]
42. Wang H, Zhang X, Xue L, Xing J, Jouvin MH, Putney JW, Anderson MP, Trebak M, and Kinet JP (2016) Low-Voltage-Activated CaV3.1 Calcium Channels Shape T Helper Cell Cytokine Profiles. Immunity 44, 782–794 [PubMed: 27037192]
43. Weinberg F, Ramnath N, and Nagrath D (2019) Reactive Oxygen Species in the Tumor Microenvironment: An Overview. Cancers (Basel) 11: 1191.
44. Hendry S, Salgado R, Gevaert T, Russell PA, John T, Thapa B, Christie M, van de Vijver K, Estrada MV, Gonzalez-Ericsson PI, Sanders M, Solomon B, Solinas C, Van den Eynden G, Allory Y, Preusser M, Hainfellner J, Pruneri G, Vingiani A, Demaria S, Symmans F, Nuciforo P, Comerma L, Thompson EA, Lakhani S, Kim SR, Schnitt S, Colpaert C, Sotiriou C, Scherer SJ, Ignatiadis M, Badve S, Pierce RH, Viale G, Sirtaine N, Penault-Llorca F, Sugie T, Fineberg S, Paik S, Srinivasan A, Richardson A, Wang Y, Chmielik E, Brock J, Johnson DB, Balko J, Wienert S, Bossuyt V, Michiels S, Ternes N, Burchardi N, Luen SJ, Savas P, Klauschen F, Watson PH, Nelson BH, Criscitiello C, O'Toole S, Larsimont D, de Wind R, Curigliano G, Andre F, Lacroix-Triki M, van de Vijver M, Rojo F, Floris G, Bedri S, Sparano J, Rimm D, Nielsen T, Kos Z, Hewitt S, Singh B, Farshid G, Loibl S, Allison KH, Tung N, Adams S, Willard-Gallo K, Horlings HM, Gandhi L, Moreira A, Hirsch F, Dieci MV, Urbanowicz M, Brcic I, Korski K, Gaire F, Koeppen H, Lo A, Giltnane J, Rebelatto MC, Steele KE, Zha J, Emancipator K, Juco JW, Denkert C, Reis-Filho J, Loi S, and Fox SB (2017) Assessing Tumor-infiltrating Lymphocytes in Solid Tumors: A Practical Review for Pathologists and Proposal for a Standardized Method From the International Immunooncology Biomarkers Working Group: Part 1: Assessing the Host Immune Response, TILs in Invasive Breast Carcinoma and Ductal Carcinoma In Situ, Metastatic Tumor Deposits and Areas for Further Research. Adv Anat Pathol 24, 235–251 [PubMed: 28777142]
45. Hendry S, Salgado R, Gevaert T, Russell PA, John T, Thapa B, Christie M, van de Vijver K, Estrada MV, Gonzalez-Ericsson PI, Sanders M, Solomon B, Solinas C, Van den Eynden G, Allory Y, Preusser M, Hainfellner J, Pruneri G, Vingiani A, Demaria S, Symmans F, Nuciforo P,

Comerma L, Thompson EA, Lakhani S, Kim SR, Schnitt S, Colpaert C, Sotiriou C, Scherer SJ, Ignatiadis M, Badve S, Pierce RH, Viale G, Sirtaine N, Penault-Llorca F, Sugie T, Fineberg S, Paik S, Srinivasan A, Richardson A, Wang Y, Chmielik E, Brock J, Johnson DB, Balko J, Wienert S, Bossuyt V, Michiels S, Ternes N, Burchardi N, Luen SJ, Savas P, Klauschen F, Watson PH, Nelson BH, Criscitiello C, O'Toole S, Larsimont D, de Wind R, Curigliano G, Andre F, Lacroix-Triki M, van de Vijver M, Rojo F, Floris G, Bedri S, Sparano J, Rimm D, Nielsen T, Kos Z, Hewitt S, Singh B, Farshid G, Loibl S, Allison KH, Tung N, Adams S, Willard-Gallo K, Horlings HM, Gandhi L, Moreira A, Hirsch F, Dieci MV, Urbanowicz M, Brcic I, Korski K, Gaire F, Koeppen H, Lo A, Giltnane J, Rebelatto MC, Steele KE, Zha J, Emancipator K, Juco JW, Denkert C, Reis-Filho J, Loi S, and Fox SB (2017) Assessing Tumor-Infiltrating Lymphocytes in Solid Tumors: A Practical Review for Pathologists and Proposal for a Standardized Method from the International Immuno-Oncology Biomarkers Working Group: Part 2: TILs in Melanoma, Gastrointestinal Tract Carcinomas, Non-Small Cell Lung Carcinoma and Mesothelioma, Endometrial and Ovarian Carcinomas, Squamous Cell Carcinoma of the Head and Neck, Genitourinary Carcinomas, and Primary Brain Tumors. Adv Anat Pathol 24, 311–335 [PubMed: 28777143]

46. Murray T, Fuertes Marraco SA, Baumgaertner P, Bordry N, Cagnon L, Donda A, Romero P, Verdeil G, and Speiser DE (2016) Very Late Antigen-1 Marks Functional Tumor-Resident CD8 T Cells and Correlates with Survival of Melanoma Patients. Front Immunol 7, 573 [PubMed: 28018343]
47. Yu P, Lee Y, Liu W, Chin RK, Wang J, Wang Y, Schietinger A, Philip M, Schreiber H, and Fu YX (2004) Priming of naive T cells inside tumors leads to eradication of established tumors. Nat Immunol 5, 141–149 [PubMed: 14704792]
48. Sawada J, Perrot CY, Chen L, Fournier-Goss AE, Oyer J, Copik A, and Komatsu M (2021) High Endothelial Venules Accelerate Naive T Cell Recruitment by Tumor Necrosis Factor-Mediated R-Ras Upregulation. Am J Pathol 191, 396–414 [PubMed: 33159887]
49. Tumeh PC, Harview CL, Yearley JH, Shintaku IP, Taylor EJ, Robert L, Chmielowski B, Spasic M, Henry G, Ciobanu V, West AN, Carmona M, Kivork C, Seja E, Cherry G, Gutierrez AJ, Grogan TR, Mateus C, Tomasic G, Glaspy JA, Emerson RO, Robins H, Pierce RH, Elashoff DA, Robert C, and Ribas A (2014) PD-1 blockade induces responses by inhibiting adaptive immune resistance. Nature 515, 568–571 [PubMed: 25428505]
50. Taube JM, Klein A, Brahmer JR, Xu H, Pan X, Kim JH, Chen L, Pardoll DM, Topalian SL, and Anders RA (2014) Association of PD-1, PD-1 ligands, and other features of the tumor immune microenvironment with response to anti-PD-1 therapy. Clinical cancer research : an official journal of the American Association for Cancer Research 20, 5064–5074 [PubMed: 24714771]
51. O'Donnell JS, Teng MWL, and Smyth MJ (2019) Cancer immunoediting and resistance to T cell-based immunotherapy. Nat Rev Clin Oncol 16, 151–167 [PubMed: 30523282]
52. Sarti P, Forte E, Mastronicola D, Giuffre A, and Arese M (2012) Cytochrome c oxidase and nitric oxide in action: molecular mechanisms and pathophysiological implications. Biochim Biophys Acta 1817, 610–619 [PubMed: 21939634]
53. Sarti P, Forte E, Giuffre A, Mastronicola D, Magnifico MC, and Arese M (2012) The Chemical Interplay between Nitric Oxide and Mitochondrial Cytochrome c Oxidase: Reactions, Effectors and Pathophysiology. Int J Cell Biol 2012, 571067
54. Borutaite V, Budriunaite A, and Brown GC (2000) Reversal of nitric oxide-, peroxynitrite- and S-nitrosothiol-induced inhibition of mitochondrial respiration or complex I activity by light and thiols. Biochim Biophys Acta 1459, 405–412 [PubMed: 11004457]
55. Zuckerbraun BS, Chin BY, Bilban M, d'Avila JC, Rao J, Billiar TR, and Otterbein LE (2007) Carbon monoxide signals via inhibition of cytochrome c oxidase and generation of mitochondrial reactive oxygen species. FASEB J 21, 1099–1106 [PubMed: 17264172]
56. Moncada S, and Bolanos JP (2006) Nitric oxide, cell bioenergetics and neurodegeneration. J Neurochem 97, 1676–1689 [PubMed: 16805776]
57. Boelens R, Wever R, Van Gelder BF, and Rademaker H (1983) An EPR study of the photodissociation reactions of oxidised cytochrome c oxidase-nitric oxide complexes. Biochim Biophys Acta 724, 176–183 [PubMed: 6309220]

58. Wang X, Tian F, Soni SS, Gonzalez-Lima F, and Liu H (2016) Interplay between up-regulation of cytochrome-c-oxidase and hemoglobin oxygenation induced by near-infrared laser. Scientific reports 6, 30540

59. Sanderson TH, Wider JM, Lee I, Reynolds CA, Liu J, Lepore B, Tousignant R, Bukowski MJ, Johnston H, Fite A, Raghunayakula S, Kamholz J, Grossman LI, Przyklenk K, and Huttemann M (2018) Inhibitory modulation of cytochrome c oxidase activity with specific near-infrared light wavelengths attenuates brain ischemia/reperfusion injury. Scientific reports 8, 3481 [PubMed: 29472564]

60. Sanderson TH, Wider JM, Lee I, Reynolds CA, Liu J, Lepore B, Tousignant R, Bukowski MJ, Johnston H, Fite A, Raghunayakula S, Kamholz J, Grossman LI, Przyklenk K, and Huttemann M (2018) Publisher Correction: Inhibitory modulation of cytochrome c oxidase activity with specific near-infrared light wavelengths attenuates brain ischemia/reperfusion injury. Scientific reports 8, 6729 [PubMed: 29695825]

61. Frossi B, De Carli M, Piemonte M, and Pucillo C (2008) Oxidative microenvironment exerts an opposite regulatory effect on cytokine production by Th1 and Th2 cells. Mol Immunol 45, 58–64 [PubMed: 17588662]

62. Kaminski MM, Sauer SW, Klemke CD, Suss D, Okun JG, Krammer PH, and Gulow K (2010) Mitochondrial reactive oxygen species control T cell activation by regulating IL-2 and IL-4 expression: mechanism of ciprofloxacin-mediated immunosuppression. J Immunol 184, 4827–4841 [PubMed: 20335530]

63. Jackson SH, Devadas S, Kwon J, Pinto LA, and Williams MS (2004) T cells express a phagocyte-type NADPH oxidase that is activated after T cell receptor stimulation. Nat Immunol 5, 818–827 [PubMed: 15258578]

64. Fu G, Xu Q, Qiu Y, Jin X, Xu T, Dong S, Wang J, Ke Y, Hu H, Cao X, Wang D, Cantor H, Gao X, and Lu L (2017) Suppression of Th17 cell differentiation by misshapen/NIK-related kinase MINK1. J Exp Med 214, 1453–1469 [PubMed: 28400474]

65. Halle S, Halle O, and Forster R (2017) Mechanisms and Dynamics of T Cell-Mediated Cytotoxicity In Vivo. Trends Immunol 38, 432–443 [PubMed: 28499492]

66. Halle S, Keyser KA, Stahl FR, Busche A, Marquardt A, Zheng X, Galla M, Heissmeyer V, Heller K, Boelter J, Wagner K, Bischoff Y, Martens R, Braun A, Werth K, Uvarovskii A, Kempf H, Meyer-Hermann M, Arens R, Kremer M, Sutter G, Messerle M, and Forster R (2016) In Vivo Killing Capacity of Cytotoxic T Cells Is Limited and Involves Dynamic Interactions and T Cell Cooperativity. Immunity 44, 233–245 [PubMed: 26872694]

67. Khan I, Tang E, and Arany P (2015) Molecular pathway of near-infrared laser phototoxicity involves ATF-4 orchestrated ER stress. Scientific reports 5, 10581

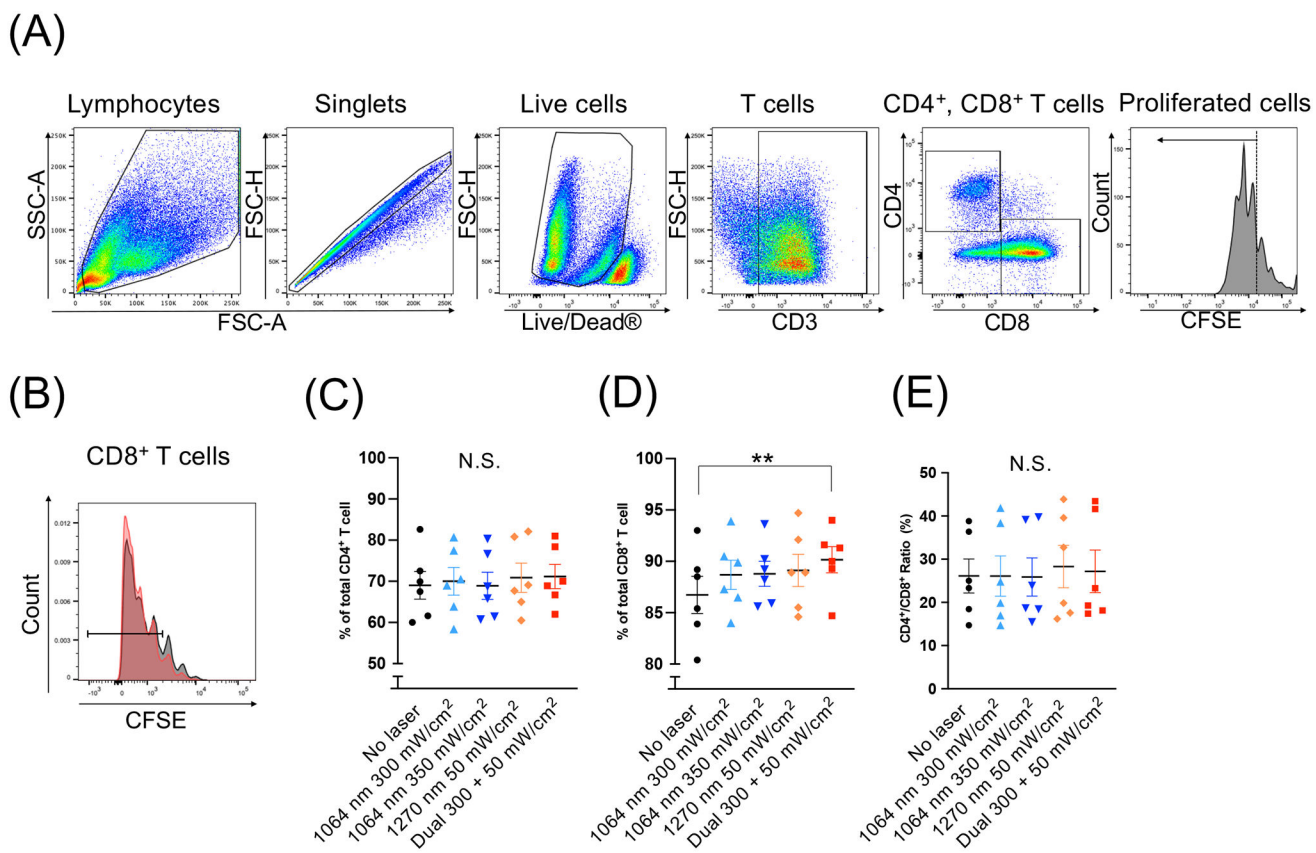

Figure 1. Dual laser illumination induced T cell proliferation *in vitro*.

Splenocytes from naive mice were labeled with CFSE and treated with near-infrared (NIR) lasers daily for 4 consecutive days in the presence of magnetic beads covalently coupled to anti-CD3 and anti-CD28 antibodies to activate T cells. On day 5, the cells were stained for CD3, CD4, CD8 and analyzed by flow cytometry. (A) Gating strategy. (B) T cell proliferation assessed by flow cytometry. Percentages of proliferated $CD4^+$ and $CD8^+$ T cells were measured. Note that dual laser treatment (red) enhanced the proliferation of $CD8^+$ T cells as compared to no laser control (gray). The percentages of (C) $CD4^+$and (D) $CD8^+$ T cells that proliferated more than three times. (E) The ratio of $CD4^+$ / $CD8^+$ T cells that proliferated more than three times. (C-E) $^{**}P < 0.01$ and *N.S.*, not significant by one-way ANOVA followed by Tukey's multiple comparisons test. $n = 6$ for each group.

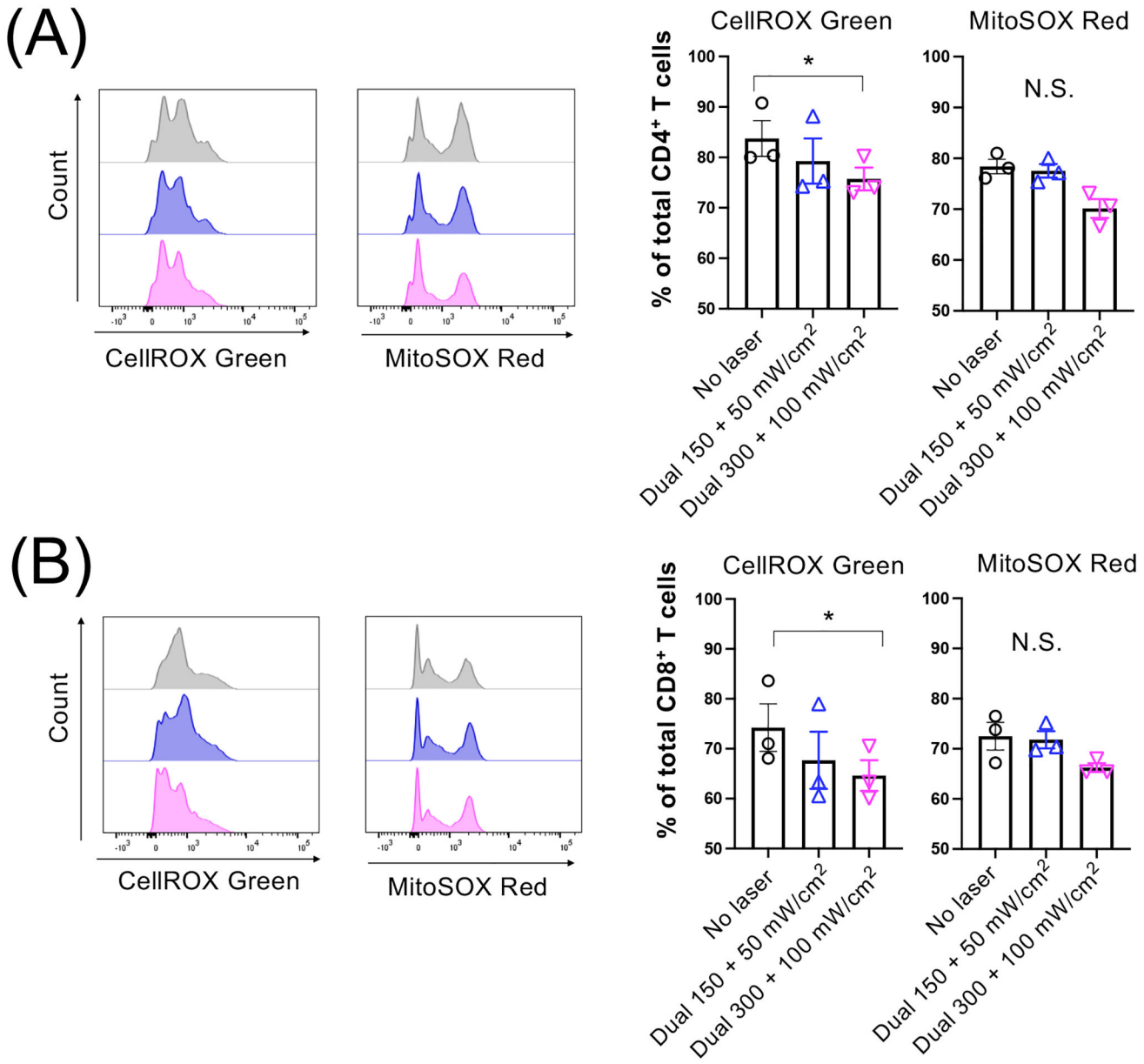

Figure 2. Dual laser illumination decreased reactive oxygen species (ROS) generation in T cells *in vitro*.

Splenocytes from naive mice were treated with dual laser (1064 nm + 1270 nm) for 1 min followed by 2 h incubation. Cells were then labeled for CD3, CD4, CD8 antibodies, incubated with CellROX Green or MitoSOX Red for 30 min, and analyzed by flow cytometry. Representative histograms and percentages of CellROX Green- and MitoSOX Red-positive (A) $CD4^+$ and (B) $CD8^+$ T cells are shown. (A-B) $n = 3$ for each group. $*P < 0.05$ by the Friedman test followed by Dunn's multiple comparisons test.

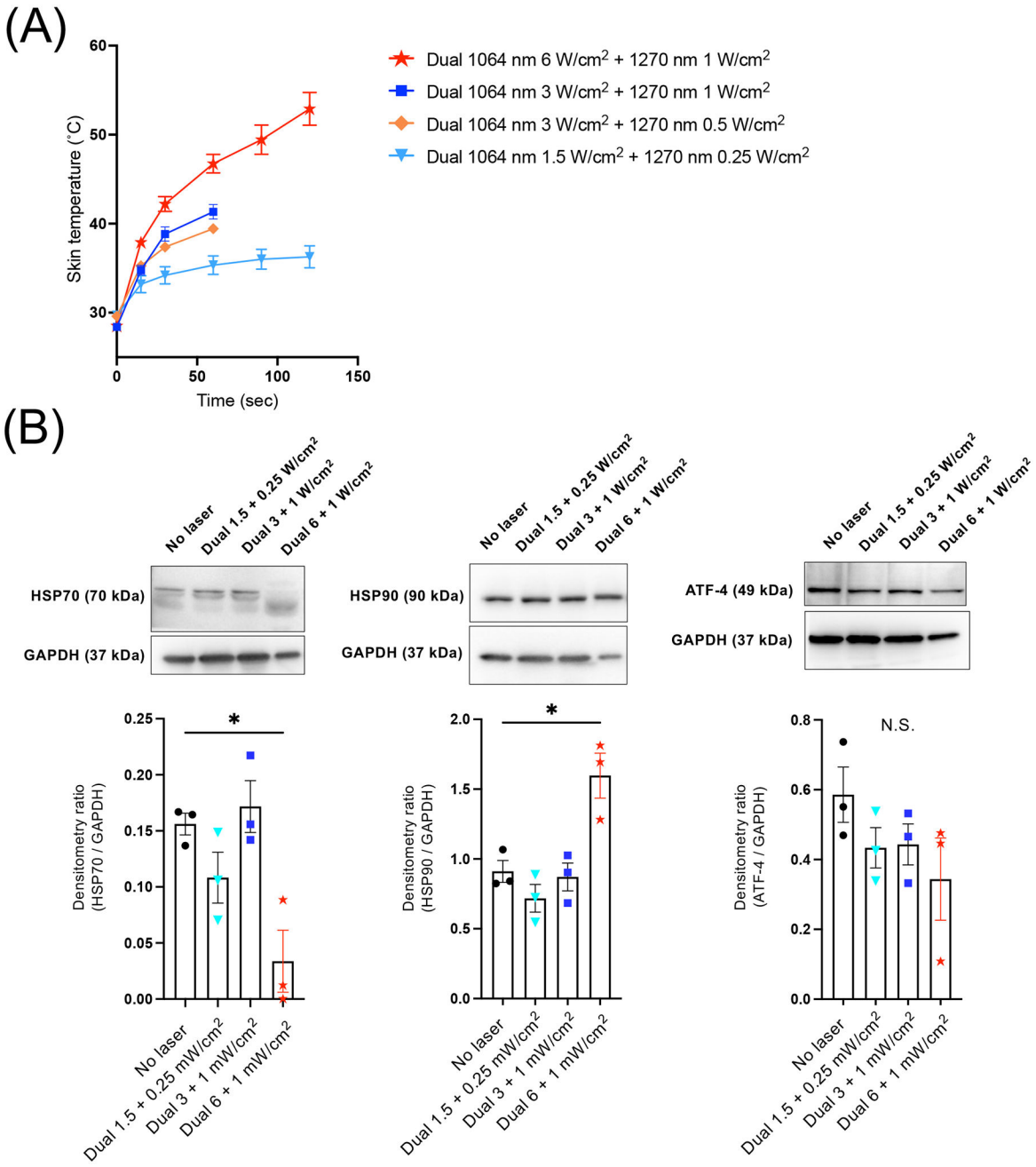

Figure 3. Safety of dual laser treatment.

(A) The depilated skin was exposed to various combinations of 1064 nm (1.5–6.0 W/cm^2) and 1270 nm (0.25–1.0 W/cm^2) NIR laser for up to 2 min. Dose-temperature responses of the dual laser treatment in mouse skin. $n=3$ for each group. Error bars show means ± s.e.m. (B) The depilated skin was exposed to various combinations of 1064 nm and 1270 nm NIR laser for 1 min. The exposed tissue was collected 24 h post-treatment and assessed by immunoblot analysis of HSP70, HSP90, and ATF-4 levels. GAPDH was used as the loading control. Top, Representative micrographs of the immunoblot analysis. Bottom, Quantitative measurements by densitometric analysis using ImageJ. Results were pooled from three

independent experiments. $n = 3$ tissue preparations for each group. **B**, Error bars denote s.e.m. A P value less than 0.05 was considered significant: * $P < 0.05$ by one-way ANOVA followed by Tukey's multiple comparison test.

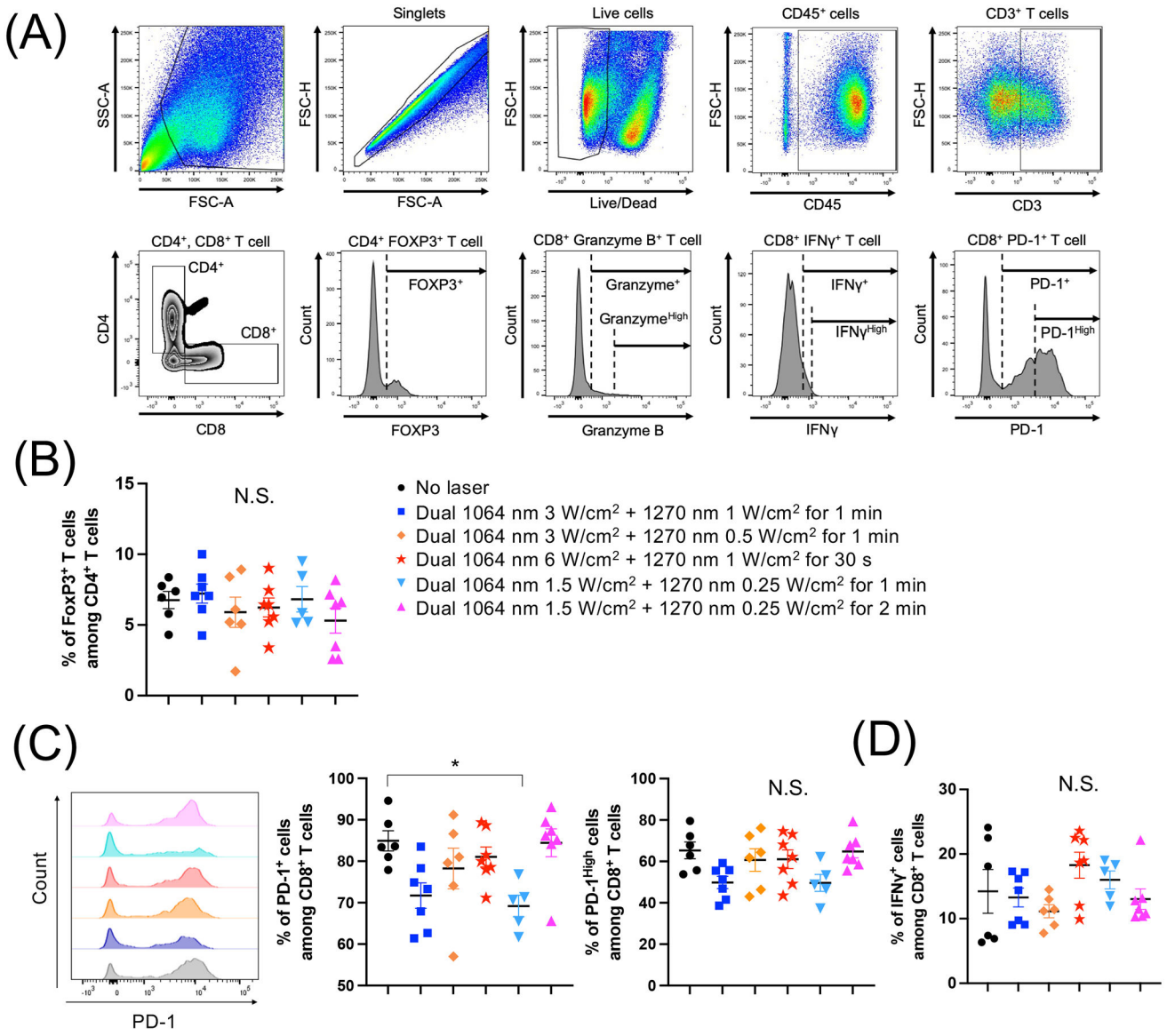

Figure 4. Dual laser treatment decreased the expression of PD-1 on tumor-infiltrating T lymphocytes (TILs).

E0771 murine breast cells were injected into the flank of C57BL/6J mice. The tumors were then treated by various combinations of 1064 nm (1.5–3 W/cm^2) and 1270 nm (0.25–1 W/cm^2) laser for 30–120 s for 5 consecutive days, from day 3 to 7. On day 16, tumor-infiltrating T lymphocytes (TILs) were purified from tumors. Single-cell suspensions of TILs were stained for surface markers and cytokines, and then analyzed by flow cytometry. (A) Gating strategy. (B) Percentages of FOXP3$^+$ CD4$^+$ T cells. (C) Representative histograms and percentages of programmed cell death protein 1 (PD-1) and (D) IFN-γ expression in CD8$^+$ T cells are shown. (A-D) n= 6, 7, 6, 7, 5, 7 for no laser, 1064 nm 3 W/cm^2 + 1270 nm 1 W/cm^2 for 1 min, 1064 nm 3 W/cm^2 + 1270 nm 0.5 W/cm^2 for 1 min, 1064 nm 6 W/cm^2 + 1270 nm 1 W/cm^2 for 30 s, 1064 nm 1.5 W/cm^2 + 1270 nm 0.25 W/cm^2 for 1 min, 1064 nm 1.5 W/cm^2 + 1270 nm 0.25 W/cm^2 for 2 min, respectively. *P < 0.05 by one-way ANOVA followed by Tukey's multiple comparisons test.

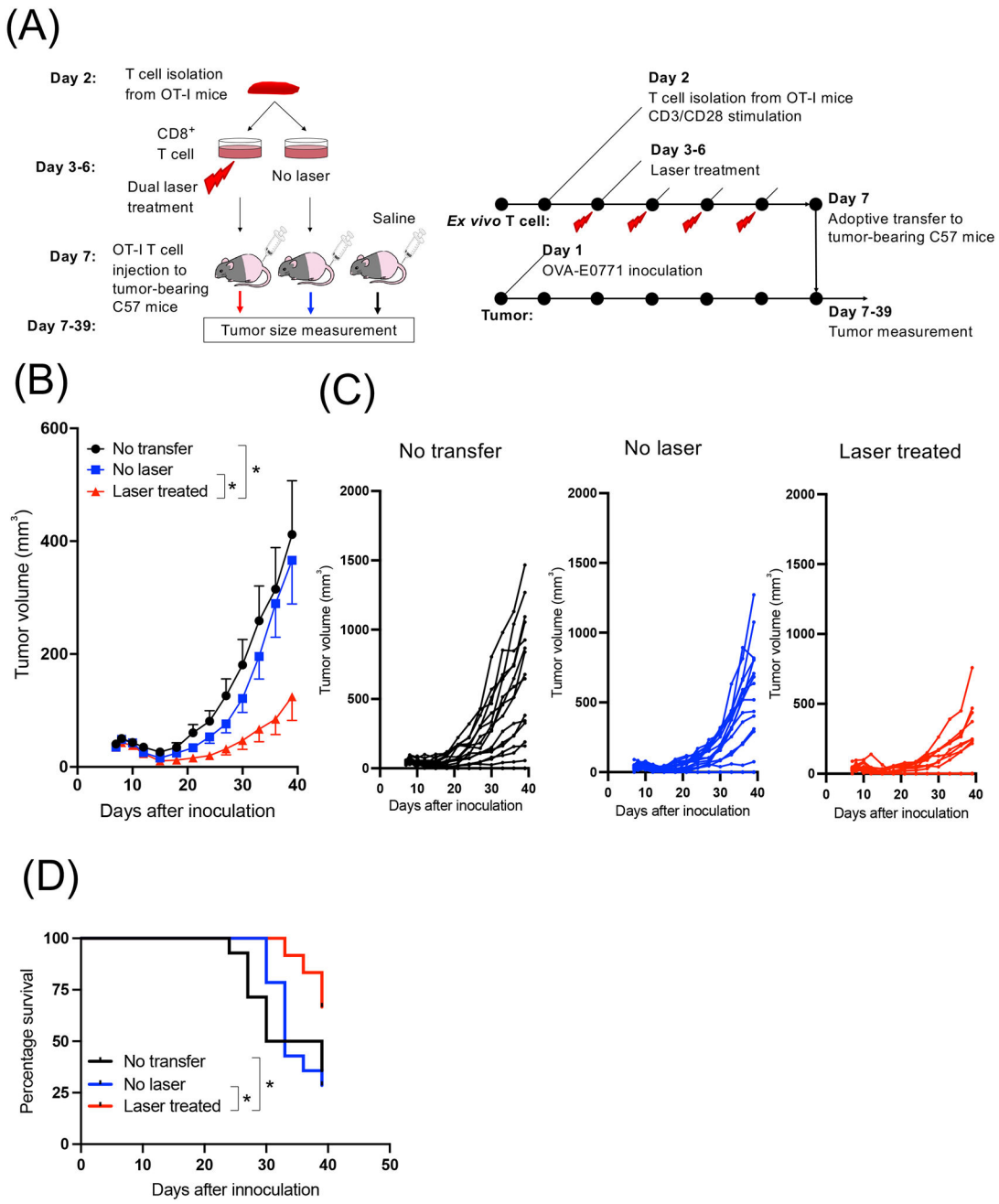

Figure 5. Dual laser treatment enhanced the efficacy of adoptive transfer therapy for a mouse model of breast cancer.

(A) A schematic demonstrating the experimental design. Splenocytes from OT-I mice were isolated and treated with the dual laser daily for 4 consecutive days in the presence of anti-CD3 and anti-CD28 antibodies *ex vivo*. On day 5, the cells were adoptively transferred to mice OVA-expressing E0771 tumors. (B) Average and (C) individual growth curves of s.c. OVA-E0771 tumors are shown. Error bars show means ± s.e.m. $n = 25, 26, 24$ for no adoptive transfer, adoptive transfer of non-laser treated cell, adoptive transfer of laser-treated cell group, respectively. $*P < 0.05$ by two-way ANOVA followed by Tukey's test. (D) Kaplan-Meier survival plots to a defined clinical endpoint (either side of tumor reached 300

mm^3 in volume) are shown. $n = 14, 14, 12$ for no adoptive transfer, adoptive transfer of non-laser treated cell, adoptive transfer of laser-treated cell group, respectively. $*P < 0.05$ by Gehan-Breslow-Wilcoxon test.

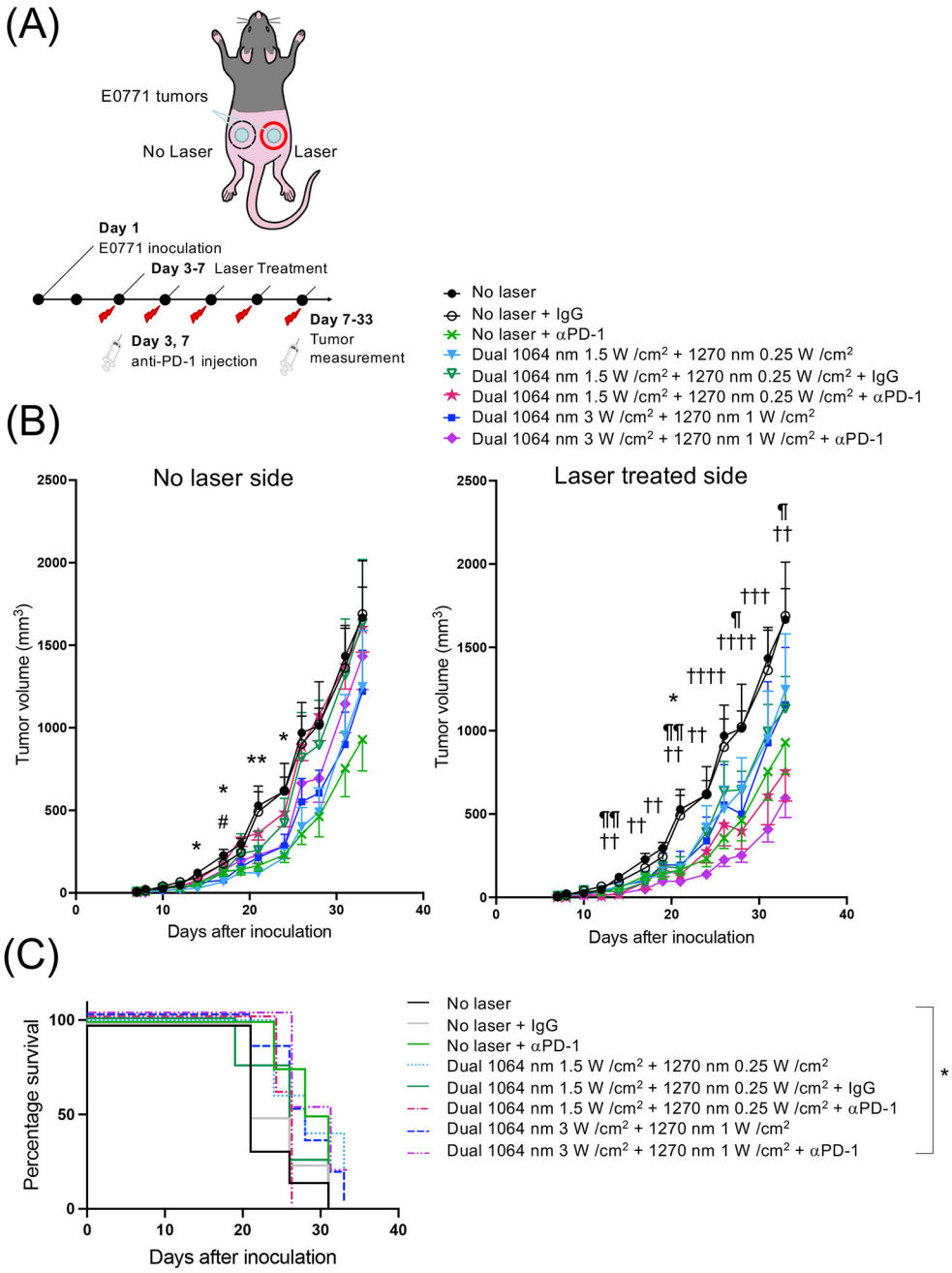

Figure 6. Dual NIR-II laser treatment enhanced the efficacy of the immune checkpoint blockade on tumor growth of a mouse model of breast cancer.

(A) A schematic showing the experimental design. E0771 murine breast cells were injected into the flank of C57BL/6J mice. The laser treatment was performed for 5 days in a row at day 3–7 at an irradiance of 1.5–3 W/cm^2 for 1064 nm laser and 0.25–1 W/cm^2 for 1270 nm laser. Anti-PD-1 antibody was injected at day 3 and 7 (100 μg each), two times in total. (B) Average growth curves of s.c. E0771 tumors in the (left) non-laser treated side and (right) laser-treated side are shown. Error bars show means ± s.e.m. n= 14, 9, 11, 5–7, 4–5, 5–7, 6–7, 7 for no laser, no laser + IgG, no laser + αPD-1, dual 1064 nm 1.5 W/cm^2 + 1270 nm 0.25 W/cm^2, dual 1064 nm 1.5 W/cm^2 + 1270 nm 0.25 W/cm^2 + IgG, dual 1064 nm

1.5 W/cm^2 + 1270 nm 0.25 W/cm^2 + αPD-1, dual 1064 nm 3 W/cm^2 + 1270 nm 1 W/cm^2, dual 1064 nm 3 W/cm^2 + 1270 nm 1 W/cm^2 + αPD-1, respectively. *$P < 0.05$, **$P < 0.01$ for no laser vs. dual 1064 nm 1.5 W/cm^2 + 1270 nm 0.25 W/cm^2; $^{\#}P < 0.05$ for no laser vs. dual 1064 nm 3 W/cm^2 + 1270 nm 1 W/cm^2, $^{¶}P < 0.05$, $^{¶¶}P < 0.01$ for no laser vs. dual 1064 nm 1.5 W/cm^2 + 1270 nm 0.25 W/cm^2 + aPD-1; $^{†}P < 0.05$, $^{††}P < 0.01$, $^{†††}P < 0.001$, $^{††††}P < 0.0001$ for no laser vs. dual 1064 nm 3 W/cm^2 + 1270 nm 1 W/cm^2 + aPD-1 groups, respectively, by two-way ANOVA with Geisser-Greenhouse correction followed by Tukey's test. (C) Kaplan-Meier survival plots to a defined clinical endpoint (either side of tumor reached at 600 mm^3 in volume) are shown. $n = 6, 4, 4, 5, 4, 5, 6, 6$ for no laser, no laser + IgG, no laser + αPD-1, dual 1064 nm 1.5 W/cm^2 + 1270 nm 0.25 W/cm^2, dual 1064 nm 1.5 W/cm^2 + 1270 nm 0.25 W/cm^2 + IgG, dual 1064 nm 1.5 W/cm^2 + 1270 nm 0.25 W/cm^2 + αPD-1, dual 1064 nm 3 W/cm^2 + 1270 nm 1 W/cm^2, dual 1064 nm 3 W/cm^2 + 1270 nm 1 W/cm^2 + αPD-1, respectively. *$P < 0.05$ by Gehan-Breslow-Wilcoxon test.

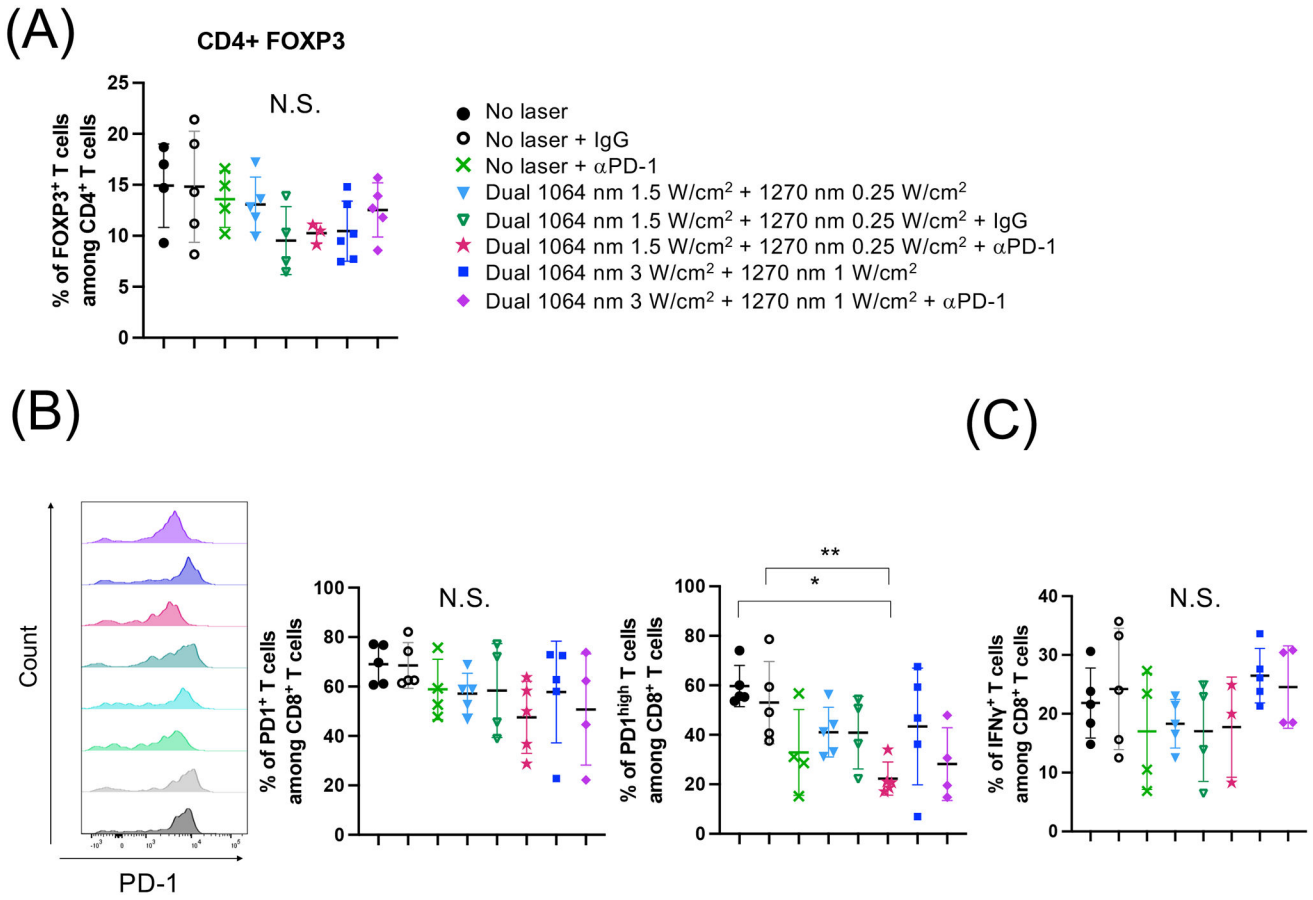

Figure 7. Dual laser treatment combined with the immune checkpoint blockade decreased the expression of PD-1 in TILs.

E0771 murine breast cells were injected into the flank of C57BL/6J mice. The laser treatment was performed for 5 days in a row at day 3–7. Anti-PD-1 antibody was injected at day 3 and 7. At day 16, TILs were purified from tumors and stained for surface markers and cytokines, and then analyzed by flow cytometry. (A) Percentages of $FOXP3^+$ $CD4^+$ T cells. (B) Representative histograms and percentages of PD-1 and (C) IFN-γ expression in $CD8^+$ T cells are shown. (A-C) n= 5, 5, 4, 5, 4, 5, 5, 4 for no laser, no laser + IgG, no laser + αPD-1, dual 1064 nm 1.5 W/cm^2 + 1270 nm 0.25 W/cm^2, dual 1064 nm 1.5 W/cm^2 + 1270 nm 0.25 W/cm^2 + IgG, dual 1064 nm 1.5 W/cm^2 + 1270 nm 0.25 W/cm^2 + αPD-1, dual 1064 nm 3 W/cm^2 + 1270 nm 1 W/cm^2, dual 1064 nm 3 W/cm^2 + 1270 nm 1 W/cm^2 + αPD-1, respectively. *P < 0.05, **P < 0.01 by one-way ANOVA followed by Tukey's multiple comparisons test.

Table 1.

Laser parameter setting.

Parameter No.	Beam spot size (cm^2)	Exposure duration (s)	1064 nm laser				1270 nm laser			
			Irradiance at target (W/cm^2)	Radiant exposure (J/cm^2)	Radiant energy (J)	Total radiant energy (J)	Irradiance at target (W/cm^2)	Radiant exposure (J/cm^2)	Radiant energy (J)	Total radiant energy (J)
1	0.32	60	0.300	18.0	5.76	23.0	-	-	-	-
2	0.32	60	0.350	21.0	6.72	26.9	-	-	-	-
3	0.32	60	-	-	-	-	0.050	3.00	0.96	3.84
4	0.32	60	0.300	18.0	5.76	23.0	0.050	3.00	0.96	3.84
5	0.32	60	0.150	9.00	2.88	11.5	0.050	3.00	0.96	3.84
6	0.32	60	0.300	18.0	5.76	23.0	0.100	6.00	1.92	7.68
7	0.20	60	3.00	180	36.0	180	1.00	60.0	12.0	60.0
8	0.20	60	3.00	180	36.0	180	0.50	30.0	6.00	30.0
9	0.20	30	6.00	180	36.0	180	1.00	30.0	6.00	30.0
10	0.20	60	1.50	90.0	18.0	90.0	0.25	15.0	3.00	15.0
11	0.20	120	1.50	180	36.0	180	0.25	30.0	6.00	30.0
12	0.20	60	3.00	180	36.0	36.0	1.00	60.0	12.0	12.0
13	0.20	60	3.00	180	36.0	36.0	0.50	30.0	6.00	6.00
14	0.20	120	1.50	180	36.0	36.0	0.25	30.0	6.00	6.00
15	0.20	120	6.00	720	144	144	1.00	120	24.0	24.0

Laser parameters used in following each experiment in this study are summarized in this Table.

Figure 1, S2: Parameter 1–4

Figure 2: Parameter 5–6

Figure 3, S3: Parameter 12–15

Figure 4, S4, S5: Parameter 7–11

Figure 5: Parameter 4

Figure 6, 7, S6, S7: Parameter 7, 10